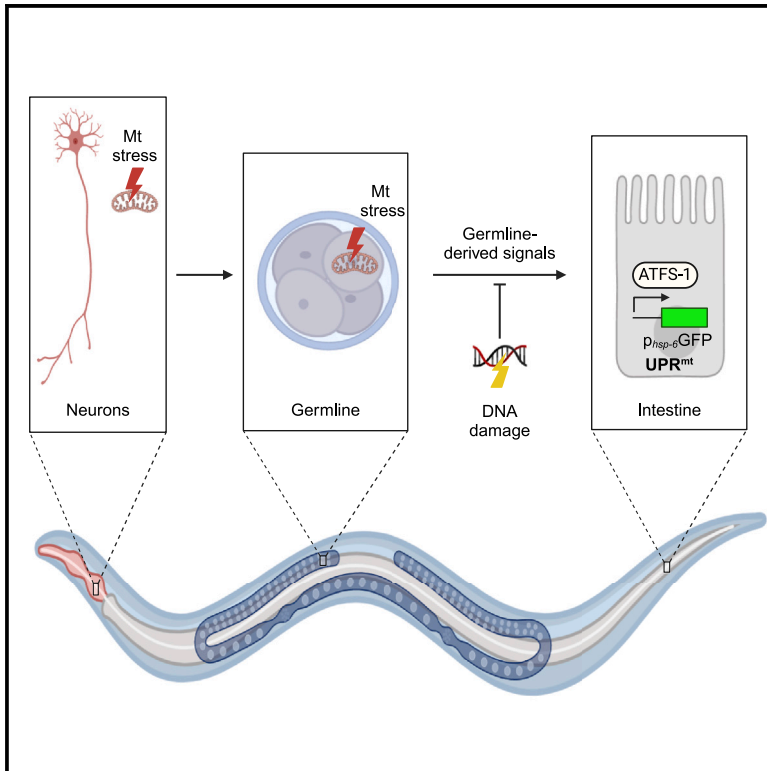


## Reproductive regulation of the mitochondrial stress response in *Caenorhabditis elegans*

### Graphical abstract



### Authors

Nikolaos Champilas, Aggeliki Sotiriou, Konstantinos Axarlis, Nektarios Tavernarakis, Thorsten Hoppe

### Correspondence

tavernarakis@imbb.forth.gr (N.T.), thorsten.hoppe@uni-koeln.de (T.H.)

### In brief

The UPR<sup>mt</sup> is a multifaceted stress response that allows cells to cope with mitochondrial stress. Champilas et al. show that an intact, reproductively active germline is essential for systemic activation of the mitochondrial stress response in a multicellular organism.

### Highlights

- UPR<sup>mt</sup> activation requires germline stem cells
- Sperm and oocyte depletion results in reduced UPR<sup>mt</sup> inducibility
- *C. elegans* males are less responsive to mitochondrial stress than hermaphrodites
- Mitochondrial stress in the germline activates UPR<sup>mt</sup> in somatic tissue



## Report

Reproductive regulation of the mitochondrial stress response in *Caenorhabditis elegans*Nikolaos Charmpilas,<sup>1,2</sup> Aggeliki Sotiriou,<sup>3,4</sup> Konstantinos Axarlis,<sup>3</sup> Nektarios Tavernarakis,<sup>3,4,\*</sup> and Thorsten Hoppe<sup>1,2,5,6,\*</sup><sup>1</sup>Institute for Genetics, University of Cologne, Cologne, Germany<sup>2</sup>Cologne Excellence Cluster on Cellular Stress Responses in Aging-Associated Diseases (CECAD), University of Cologne, Cologne, Germany<sup>3</sup>Institute of Molecular Biology and Biotechnology, Foundation for Research and Technology-Hellas, Heraklion, Greece<sup>4</sup>Division of Basic Sciences, School of Medicine, University of Crete, Heraklion, Greece<sup>5</sup>Center for Molecular Medicine Cologne (CMMC), Faculty of Medicine and University Hospital of Cologne, Cologne, Germany<sup>6</sup>Lead contact\*Correspondence: [tavernarakis@imbb.forth.gr](mailto:tavernarakis@imbb.forth.gr) (N.T.), [thorsten.hoppe@uni-koeln.de](mailto:thorsten.hoppe@uni-koeln.de) (T.H.)<https://doi.org/10.1016/j.celrep.2024.114336>

## SUMMARY

Proteome integrity is fundamental for cellular and organismal homeostasis. The mitochondrial unfolded protein response (UPR<sup>mt</sup>), a key component of the proteostasis network, is activated in a non-cell-autonomous manner in response to mitochondrial stress in distal tissues. However, the importance of inter-tissue communication for UPR<sup>mt</sup> inducibility under physiological conditions remains elusive. Here, we show that an intact germline is essential for robust UPR<sup>mt</sup> induction in the *Caenorhabditis elegans* somatic tissues. A series of nematode mutants with germline defects are unable to respond to genetic or chemical UPR<sup>mt</sup> inducers. Our genetic analysis suggests that reproductive signals, rather than germline stem cells, are responsible for somatic UPR<sup>mt</sup> induction. Consistent with this observation, we show that UPR<sup>mt</sup> is sexually dimorphic, as male nematodes are inherently unresponsive to mitochondrial stress. Our findings highlight a paradigm of germline-somatic communication and suggest that reproductive cessation is a primary cause of age-related UPR<sup>mt</sup> decline.

## INTRODUCTION

Loss of protein homeostasis (proteostasis) is a hallmark of aging and has been implicated in several human pathologies, collectively termed proteinopathies.<sup>1</sup> The proteostasis network (PN), an extensive chaperone network supported by stress response pathways and the protein degradation machinery, prevents the accumulation of damaged proteins, toxic oligomers, and protein aggregates.<sup>2,3</sup> Landmark studies in the nematode *Caenorhabditis elegans* demonstrated that proteostasis decline is an early, programmed event rather than a consequence of aging. Interestingly, genetic interventions that extend the lifespan, such as inhibition of insulin/IGF-1 signaling, can delay the onset of proteostasis decline.<sup>4,5</sup> Intense scientific efforts have focused on elucidating the molecular basis of PN regulation in order to rescue cells and organisms from the consequences of age-associated proteostasis decline.

The mitochondrial unfolded protein response (UPR<sup>mt</sup>) is activated by stressors that inhibit oxidative phosphorylation and pathogen attack. In addition, the UPR<sup>mt</sup> senses stoichiometric imbalances of electron transport chain (ETC) complexes caused by reduced mitochondrial protein synthesis or impaired transport of nuclear-encoded ETC components into mitochondria.<sup>6–8</sup> Central to UPR<sup>mt</sup> activation is ATFS-1, a basic leucine zipper transcription factor that harbors both a mitochondrial and a nu-

clear localization signal. Under basal conditions, ATFS-1 is imported into the mitochondria and degraded.<sup>9</sup> However, upon mitochondrial challenge, ATFS-1 is stabilized and translocates to the nucleus, where it activates a broad transcriptional program to restore mitochondrial proteostasis, rewire metabolism, and enhance innate immunity.<sup>10,11</sup> In addition to ATFS-1, UPR<sup>mt</sup> activation relies on the homeobox transcription factor DVE-1, the deubiquitylase UBL-5, the sphingosine kinase SPHK-1, and several epigenetic chromatin regulators.<sup>12–18</sup> In mammals, accumulating evidence suggests that the transcription factors ATF-4, and ATF-5, which are preferentially translated upon activation of the integrated stress response, are involved in UPR<sup>mt</sup> induction.<sup>19–21</sup> Extensive studies have shown that mitochondrial stress in neurons activates the UPR<sup>mt</sup> in a non-cell-autonomous manner.<sup>22–25</sup> However, the importance of inter-tissue communication for UPR<sup>mt</sup> induction under physiological conditions remains largely elusive.

In this study, we propose that germline-derived signals are essential for robust UPR<sup>mt</sup> activation in *C. elegans* somatic tissues under mitochondrial stress. We performed a genetic analysis, in which we depleted individual germline populations, such as germline stem cells, sperm, and oocytes, and uncovered a direct link between reproduction and somatic UPR<sup>mt</sup> induction. Consistently, we show that the two sexes of *C. elegans* respond differently to mitochondrial stress. Our results demonstrate that



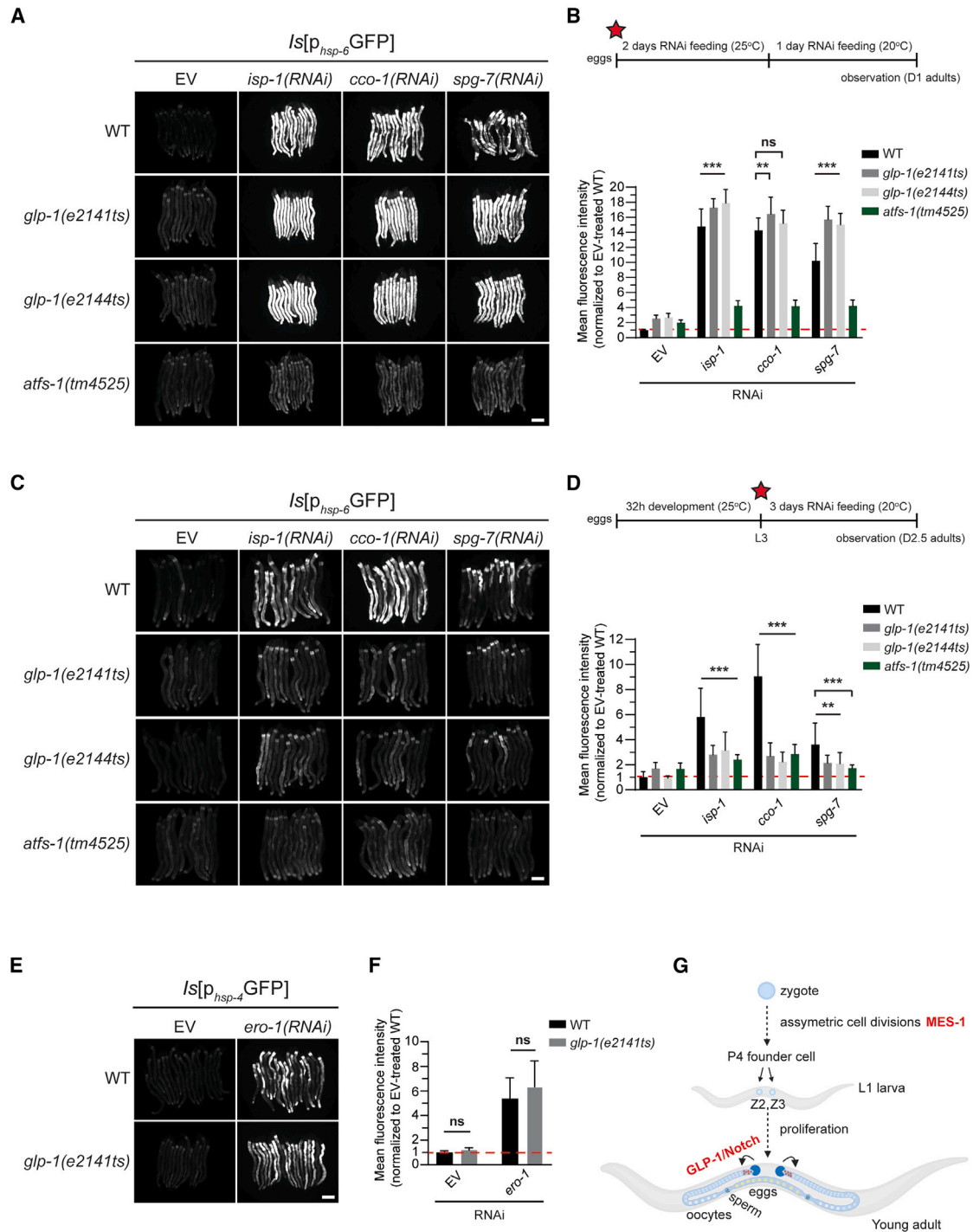


**Figure 1. An intact GSC pool is required for somatic UPR<sup>mt</sup> induction**

(A) Photomicrographs of day 1 adult wild-type (WT), *glp-1(e2141ts)*, *glp-1(e2144ts)*, and *atfs-1(tm4525)* mutant  $p_{hsp-6}GFP$  reporter nematodes treated with empty vector (EV) and three UPR<sup>mt</sup>-inducing RNAs from hatching.

(B) Quantification of intestinal  $p_{hsp-6}GFP$  fluorescence in WT, *glp-1(e2141ts)*, *glp-1(e2144ts)*, and *atfs-1(tm4525)* mutants ( $n = 3$ , \*\*\* $p < 0.001$ , \*\* $p < 0.01$ , two-way ANOVA). The red stars signify the time point when mitochondrial stress was administered.

(C) Photomicrographs of day 3 adult WT, *glp-1(e2141ts)*, *glp-1(e2144ts)*, and *atfs-1(tm4525)* mutant  $p_{hsp-6}GFP$  reporter nematodes treated with EV and three UPR<sup>mt</sup>-inducing RNAs from the L3 larval stage.

(D) Quantification of  $p_{hsp-6}GFP$  fluorescence in WT, *glp-1(e2141ts)*, *glp-1(e2144ts)*, and *atfs-1(tm4525)* mutants ( $n = 3$ , \*\*\* $p < 0.001$ , \*\* $p < 0.01$ , two-way ANOVA).

(E) Photomicrographs of day 3 adult WT and *glp-1(e2141ts)* mutant  $p_{hsp-4}GFP$  reporter nematodes treated with EV and *ero-1(RNAi)* from the L4 larval stage.

(legend continued on next page)

germline-to-soma signaling regulates a central stress response and that reproductive diapause correlates with the age-related decline in somatic proteostasis.

## RESULTS

### Somatic UPR<sup>mt</sup> induction requires germline stem cell proliferation

Gamete production is an energy-demanding process that is highly dependent on mitochondrial function.<sup>26</sup> We hypothesized that changes in germline homeostasis could be transmitted to the soma and affect the UPR<sup>mt</sup>. To address this, we used two temperature-sensitive (ts) mutants for the *glp-1* gene, which encodes the worm Notch receptor homolog, to achieve ablation of the reproductive germline<sup>27</sup>. GLP-1(Notch) signaling is essential for the renewal of germline stem cells (GSCs), which give rise to all gametes in the hermaphrodite gonads of *C. elegans*.<sup>28</sup> When *glp-1(ts)* mutants are raised at the restrictive temperature (25°C), their GSCs are progressively depleted, eventually producing germline-less, sterile nematodes.<sup>29</sup> To assess UPR<sup>mt</sup> activation, we used a transgenic strain expressing GFP under the control of the promoter of *hsp-6* (*p<sub>hsp-6</sub>*-GFP), a mitochondrial Hsp70 chaperone that is robustly induced upon mitochondrial stress, predominantly in the intestine.<sup>30</sup> We kept the duration of mitochondrial stress constant (three consecutive days) and varied the time of initial stress application. When *glp-1(e2141ts)* and *glp-1(e2144ts)* mutants were challenged from hatching by RNAi-mediated inhibition of *isp-1*, *cco-1*, and *spg-7*, which are known to trigger the UPR<sup>mt</sup>, they were able to induce *p<sub>hsp-6</sub>*-GFP expression, similar to their wild-type counterparts, although their GSCs were progressively eliminated by the onset of adulthood (Figures 1A and 1B). Thus, mitochondrial challenge prior to GSC depletion robustly induced the UPR<sup>mt</sup>. However, when mitochondrial stress was first applied 32 h after egg laying, a time point corresponding to the L3 larval stage when the developmental temperature is set at 25°C, both *glp-1* mutants failed to induce *p<sub>hsp-6</sub>*-GFP and were reminiscent of the *atfs-1(tm4525)* null mutants, which are inherently UPR<sup>mt</sup> unresponsive (Figures 1C and 1D). At 15°C (permissive temperature), *glp-1(e2141ts)* mutants are fertile, indistinguishable from wild-type worms, and responsive to *atp-3* knockdown, which induces the UPR<sup>mt</sup> through formation of the mitochondrial permeability transition pore<sup>31</sup> (Figures S1A and S1B). This was reversed when the animals were grown at 25°C (restrictive temperature) (Figures S1C and S1D). Thus, UPR<sup>mt</sup> induction correlates with the penetrance of the *glp-1(e2141ts)* mutation. As an alternative to RNAi feeding, we stressed worms with antimycin A, a mitochondrial toxin produced by *Streptomyces* spp. and a potent UPR<sup>mt</sup> inducer.<sup>32,33</sup> We observed that the inducibility of *p<sub>hsp-6</sub>*-GFP expression was impaired in *glp-1(e2141ts)* mutants (Figure S1E). *glp-1* mutants are long lived, and this is dependent on the activation of the DAF-16/FoxO transcription fac-

tor.<sup>34</sup> However, *daf-16(mu86); glp-1(e2141ts)* double mutants behaved similarly to *glp-1(e2141ts)* single mutants upon antimycin A treatment, demonstrating that GSC-depleted animals are unable to induce the UPR<sup>mt</sup> independent of DAF-16/FoxO (Figure S1F).

We obtained similar results when mitochondrial stress was first applied at the L4 larval stage. To corroborate our findings, we also analyzed *glp-4(bn2ts)* mutants, which produce only a small number of mitosis-arrested germline nuclei when grown at the restrictive temperature.<sup>35,36</sup> Similar to *glp-1(e2144ts)*, *glp-4(bn2ts)* mutants failed to robustly induce *p<sub>hsp-6</sub>*-GFP expression upon treatment with UPR<sup>mt</sup> RNAi inducers from the L4 larval stage (Figures S2A and S2B) and upon antimycin A treatment (Figures S2C and S2D). Notably, the development of *glp-4(bn2ts)* mutants was delayed upon challenge with *spg-7(RNAi)* (Figures S2E and S2F). We next asked whether GSC elimination affects the ability of nematodes to activate other stress pathways. The endoplasmic reticulum (ER) UPR (UPR<sup>ER</sup>), which is activated when the ER protein folding capacity is compromised, reduces the load of unfolded proteins in the ER.<sup>37</sup> Expression of the chaperone HSP-4 has been widely used as a reliable marker of UPR<sup>ER</sup> activation.<sup>38</sup> We found that *glp-1(e2141ts)* mutants could induce *p<sub>hsp-4</sub>*-GFP expression to wild-type levels upon knockdown of the ER oxidoreductase *ero-1* (Figures 1E and 1F). These results indicate that GSC elimination renders germline-less mutants less responsive specifically to UPR<sup>mt</sup>-inducing insults.

### An intact germline is a prerequisite for somatic UPR<sup>mt</sup> activation

We asked whether the absence of active GSC proliferation in germline-less mutants accounts for their reduced ability to induce the UPR<sup>mt</sup>. In contrast to *glp-1* loss-of-function mutants, *glp-1(ar202)* gain-of-function mutants exhibit a hyperproliferative phenotype manifested by the formation of proximal gonadal arm tumors with abundant mitotic nuclei (Figure S3A).<sup>39</sup> We reasoned that, if GSC depletion abolishes UPR<sup>mt</sup> induction, then mitochondrial stress applied to the *glp-1(ar202)* mutants would induce an equal or even stronger UPR<sup>mt</sup>. However, *glp-1(ar202)* mutants failed to mount a robust UPR<sup>mt</sup> upon antimycin A treatment (Figures S3B and S3C). Thus, impairment of a process other than GSC proliferation attenuates the potential of germline-less mutants to mount a robust UPR<sup>mt</sup>. The germline is a tissue of active mtDNA replication associated with progeny production. Lack of GSC proliferation results in reduced mtDNA copy numbers.<sup>40</sup> However, knockdown of *polg-1/POLG*, the RNA polymerase involved in mtDNA replication,<sup>41</sup> did not affect UPR<sup>mt</sup> induction upon antimycin A treatment (Figures S3D and S3E). This suggests that mtDNA copy number does not correlate with UPR<sup>mt</sup> induction.

During embryogenesis, three rounds of cell division of the P2 blastomere of the four-cell stage embryo generate the P4 germline founder cell. P4 division gives rise to two primordial germ

(F) Quantification of *p<sub>hsp-4</sub>*-GFP fluorescence in WT and *glp-1(e2141ts)* upon EV and *ero-1(RNAi)* treatments ( $n > 3$ ;  $p > 0.05$ ; two-way ANOVA).

(G) Overview of *C. elegans* germline development. Asymmetric divisions of the zygote specify the P4 founder cell, which divides once more to produce the two primordial germ cells (PGCs) Z2 and Z3. PGCs proliferate during the larval stages, giving rise to the two mature, U-shaped hermaphrodite gonads.

Data are represented as mean  $\pm$  SD. Scale bars, 200  $\mu$ m.

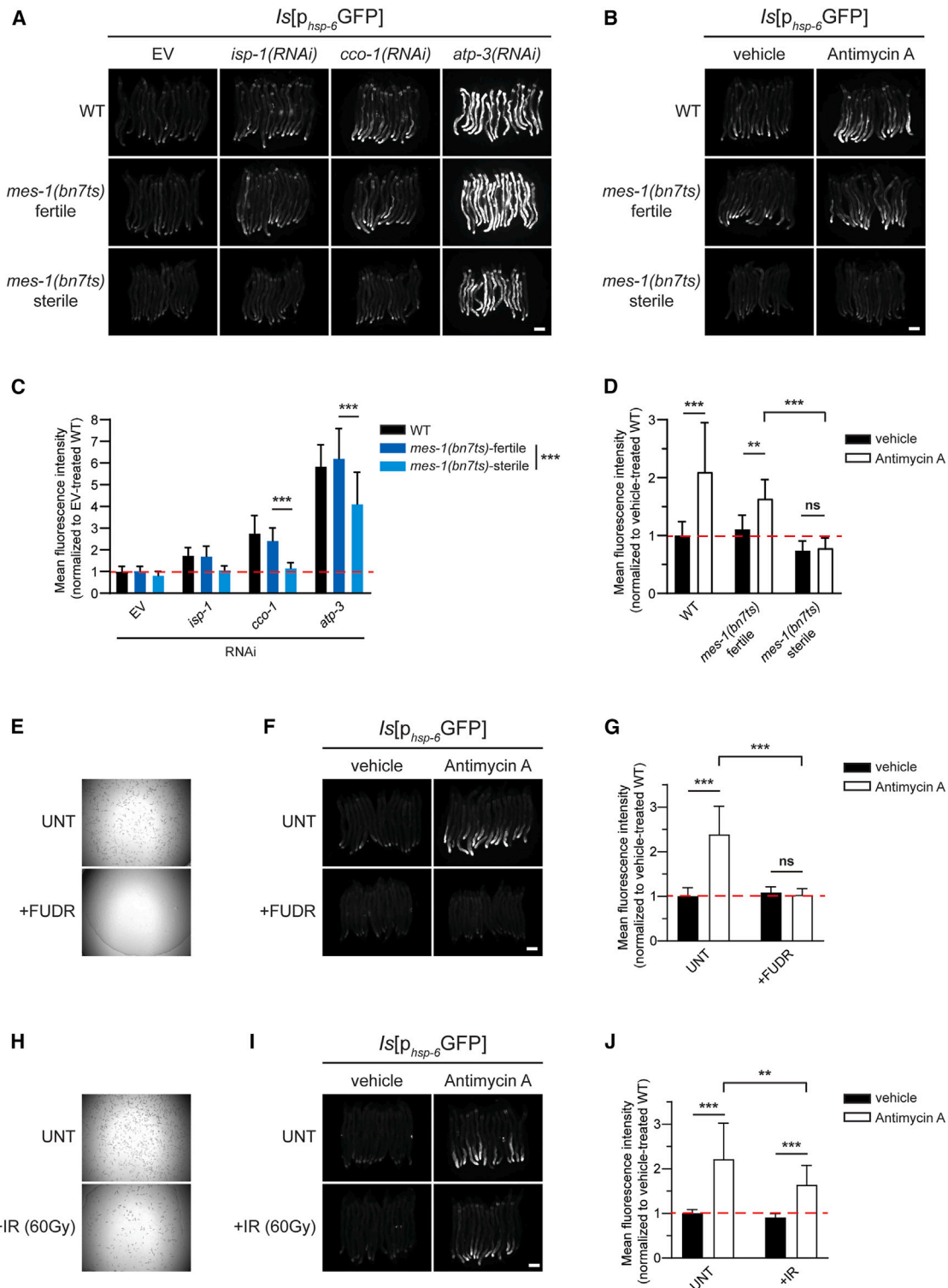


**Figure 2. The germline is essential for full-scale UPR<sup>mt</sup> induction**

(A) Photomicrographs of day 3 adult WT and *mes-1(bn7ts)* mutant *p<sub>hsp-6</sub>GFP* reporter nematodes treated with EV, *isp-1(RNAi)*, *cco-1(RNAi)*, and *atp-3(RNAi)* from the L4 larval stage.

(B) Photomicrographs of day 2 adult WT and *mes-1(bn7ts)* mutant *p<sub>hsp-6</sub>GFP* reporter nematodes treated with antimycin A.

(C) Quantification of *p<sub>hsp-6</sub>GFP* fluorescence intensity in WT and *mes-1(bn7ts)* mutants. Treatments were the same as in (A) ( $n = 3$ ,  $***p < 0.001$ , two-way ANOVA).

(D) Quantification of *p<sub>hsp-6</sub>GFP* fluorescence in WT and *mes-1(bn7ts)* mutants upon antimycin A treatment ( $n = 3$ ,  $***p < 0.001$ ,  $**p < 0.01$ , two-way ANOVA).

(legend continued on next page)

cells, Z2 and Z3, which begin to proliferate after hatching to form to the entire germline (Figure 1G).<sup>42</sup> *mes-1(bn7ts)* mutants show defects in asymmetric cell divisions, resulting in the transformation of P4 into a muscle progenitor.<sup>43</sup> Consequently, almost half of the progeny produced by *mes-1(bn7ts)* homozygous hermaphrodites are sterile, while the rest of the population remains fertile, due to the incomplete penetrance of the *mes-1(bn7)* mutation. Interestingly, sterile *mes-1(bn7ts)* mutant animals failed to induce  $p_{hsp-6}$ -GFP expression to wild-type levels upon *isp-1*, *cco-1* and *atp-3* knockdown or antimycin A treatment, while their fertile, genetically identical siblings responded reminiscent of the wild type (Figures 2A–2D). To assess whether somatic gonad development could affect the somatic UPR<sup>mt</sup>, we used mutants for *gon-2*, which is involved in the division of somatic gonad progenitors.<sup>44</sup> We found that *gon-2(q388ts)* mutants also failed to induce UPR<sup>mt</sup> upon ETC inhibition (Figures S4A–S4D). We verified these findings by monitoring  $p_{hsp-6}$ -GFP reporter induction with an anti-GFP antibody under normal conditions and after antimycin A treatment (Figure S4E).

At the end of development, *C. elegans* somatic cells are terminally differentiated and post mitotic. The germline is the only tissue where active cell division occurs in the adult *C. elegans*. Since our results indicated that the reproductive status determines the potential of the soma to induce the UPR<sup>mt</sup>, we wondered what the effect of stress, which predominantly affects germline cells, would be on the somatic UPR<sup>mt</sup>. We used 5-fluoro-2'-deoxyuridine (FUDR), which intercalates into DNA strands, causing replication arrest. A 24-h FUDR treatment produced sterile nematodes that failed to induce UPR<sup>mt</sup> following antimycin A challenge (Figures 2E–2G). We also applied ionizing radiation (IR), which induces DNA double-strand break formation and germline apoptosis.<sup>45</sup> Exposure to an intermediate dose of IR reduced brood size and attenuated  $p_{hsp-6}$ -GFP induction upon antimycin A treatment (Figures 2H–2J). Ultraviolet B (UV-B) radiation leads to the formation of cyclobutene-pyrimidine dimers and photoproducts.<sup>46</sup> Increasing doses of UV-B reduced brood size and UPR<sup>mt</sup> induction in the soma (Figures S4F–S4H).

We extended our analysis to a non-cell-autonomous UPR<sup>mt</sup> induction paradigm. Neuronal overexpression of a polyglutamine tract of 40 glutamines (Q40) is known to induce UPR<sup>mt</sup> non-cell autonomously.<sup>23</sup> Interestingly, the induction of  $p_{hsp-6}$ -GFP in the posterior intestine was weaker when these animals were grown on FUDR plates (Figures S5A and S5B). The same was true when we compared wild-type animals and *glp-1(e2141ts)* mutants in the presence of pan-neuronal Q40 (Figures S5C and S5D). Thus, an actively proliferating, intact germline is essential for full UPR<sup>mt</sup> inducibility in response to various insults.

### Active reproduction is associated with somatic UPR<sup>mt</sup> induction

Next, we investigated whether the absence of germline populations other than mitotic GSCs could undermine somatic UPR<sup>mt</sup> inducibility. To this end, we took advantage of *ts* mutants for the sex determination pathway.<sup>47</sup> We observed that *fem-1(hc17ts)* mutants, which become feminized when raised at 25°C, retained only a residual potential to induce UPR<sup>mt</sup>, albeit significantly weaker than wild-type worms (Figures 3A and 3B). Oogenesis-defective *fem-3(q20gof)* mutants, which produce excess sperm at the expense of oocytes, failed to induce the mitochondrial stress response upon ETC inhibition (Figures S6A and S6B). Thus, the absence of sperm alone cannot explain the reduced UPR<sup>mt</sup> inducibility. Furthermore, sperm- and oocyte-deficient mutants remained unresponsive to antimycin A, phenocopying germline-less mutants (Figures S6C and S6D). We validated these findings by quantifying GFP expression in hundreds of worms using the Copas biosorter (Figure S6E) and by western blotting with an anti-GFP antibody (Figure S6F). Interestingly, mating of feminized *fem-1(hc17ts)* mutants with wild-type males partially restores  $p_{hsp-6}$ -GFP induction upon antimycin A treatment, along with their ability to produce viable offspring. This is independent of male pheromone production, as mating with *daf-22(m130)* males, which are inherently defective in pheromone biosynthesis,<sup>48</sup> could also restore UPR<sup>mt</sup> inducibility of sperm-deficient nematodes (Figures 3C and 3D). Taken together, these results demonstrate that the ability to reproduce is a prerequisite for full somatic UPR<sup>mt</sup> induction.

Next, we asked whether sperm or oocyte deficiency leads to generalized stress response defects. To this end, we crossed sperm- and oocyte-deficient mutants with established stress response reporters. Treatment with tunicamycin, an inhibitor of N-glycosylation and potent UPR<sup>ER</sup> inducer, induced  $p_{hsp-4}$ -GFP expression in both *fem-1(hc17ts)* and *fem-3(q20gof)* mutants (Figures S7A and S7B). Another key player in proteostasis is the transcription factor HSF-1, the master regulator of the heat shock response (HSR).<sup>49</sup> The *hsp20/alpha-B-crystallin* family member *hsp-16.2*, whose expression is induced upon heat shock,<sup>50</sup> is a transcriptional target of HSF-1.<sup>51</sup> Both feminized and masculinized mutants induced  $p_{hsp-16.2}$ -GFP expression close to wild-type levels upon heat stress (Figures S7C and S7D). In addition to exogenous insults, cells often face endogenous stress caused by reactive oxygen species, byproducts of cellular metabolism that damage vital cellular macromolecules. SKN-1/Nrf2 orchestrates the oxidative stress response (OxSR)<sup>52</sup> by transcribing numerous genes, such as *gst-4*.<sup>53</sup> *Fem-1(hc17ts)* and *fem-3(q20gof)* mutants could induce *gst-4* expression upon treatment with paraquat, a superoxide radical generator (Figures S7E and S7F). Taken together, among the major stress responses, only the UPR<sup>mt</sup> is impaired when reproduction ceases due to the lack of sperm or oocytes.

(E) A 24-h FUDR treatment produces sterile nematodes. UNT, untreated.

(F) Photomicrographs of day 2 adult WT  $p_{hsp-6}$ -GFP reporter nematodes grown on standard or FUDR-containing plates before antimycin A challenge.

(G) Quantification of  $p_{hsp-6}$ -GFP fluorescence upon antimycin A challenge in untreated and FUDR-treated animals ( $n = 3$ , \*\*\* $p < 0.001$ , two-way ANOVA).

(H) An intermediate ionizing radiation (IR) dose reduces brood size.

(I) Photomicrographs of day 2 adult WT  $p_{hsp-6}$ -GFP reporter nematodes exposed to a 60-Gy IR dose before antimycin A challenge.

(J) Quantification of  $p_{hsp-6}$ -GFP fluorescence upon antimycin A challenge in untreated and IR-treated animals ( $n = 3$ , \*\*\* $p < 0.001$ , \*\* $p < 0.01$ , two-way ANOVA).

Data are represented as mean  $\pm$  SD. Scale bars, 200  $\mu$ m.

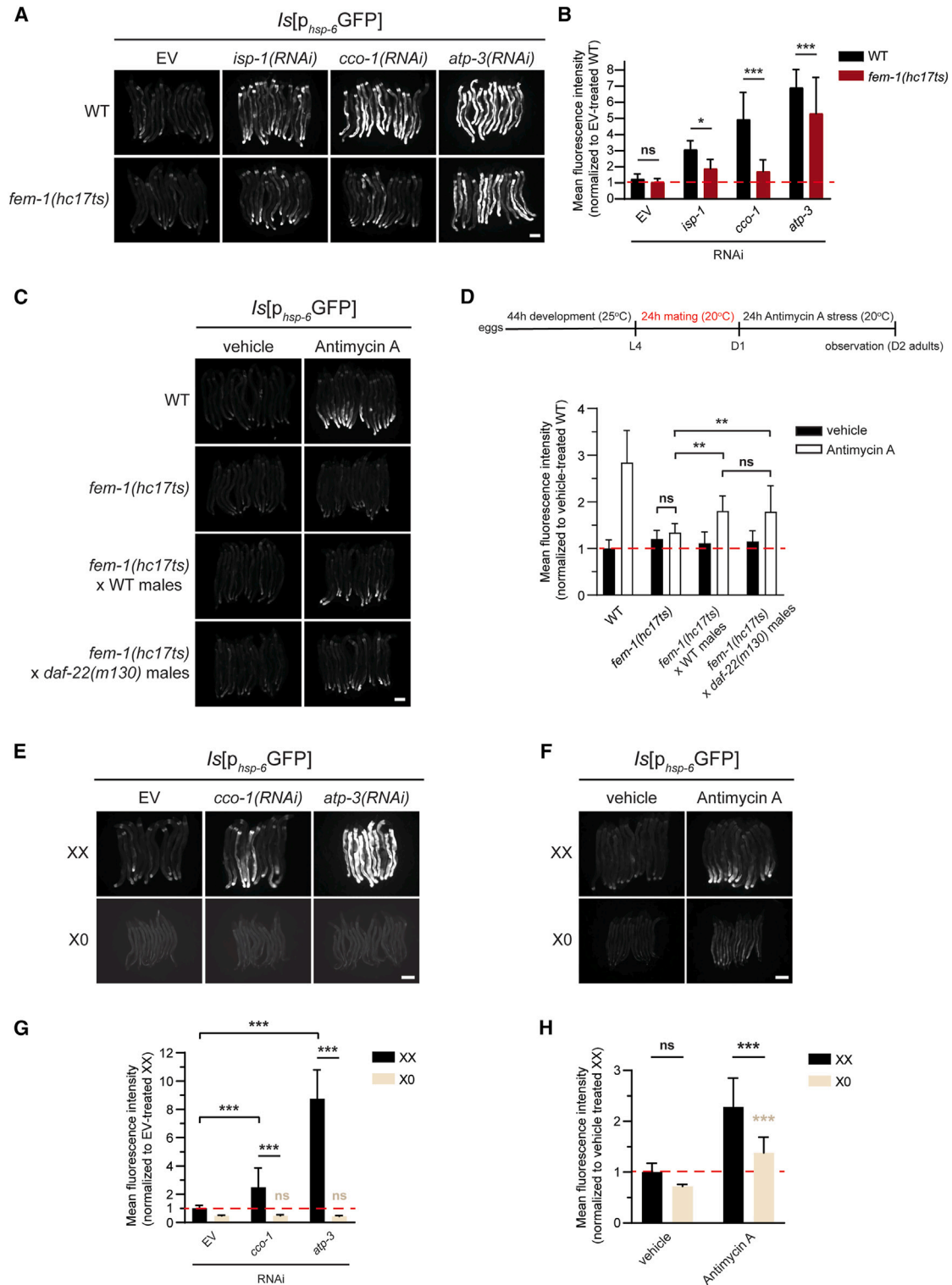


**Figure 3. Reproduction is coupled with somatic UPR<sup>mt</sup>**

(A) Photomicrographs of day 3 adult WT and *fem-1(hc17ts)* mutant *p<sub>hsp-6</sub>GFP* reporter nematodes treated with EV and three UPR<sup>mt</sup>-inducing RNAis from the L4 larval stage.

(B) Quantification of intestinal *p<sub>hsp-6</sub>GFP* fluorescence in WT and feminized mutants ( $n > 3$ , \*\*\* $p < 0.001$ , \* $p < 0.05$ , two-way ANOVA).

(legend continued on next page)

The finding that oocyte production is essential for full-scale UPR<sup>mt</sup> induction in the soma led us to hypothesize that there may be a differential potential for UPR<sup>mt</sup> induction between the two sexes. The nematode *C. elegans* exists in nature primarily as a hermaphrodite with two sex chromosomes (XX), producing both sperm and oocytes from a common pool of GSCs. Males with a single sex chromosome (X0) arise randomly at low frequencies due to meiotic nondisjunction events. While genetic inhibition of *cco-1* and *atp-3* induced p<sub>hsp-6</sub>-GFP expression in hermaphrodites, it failed to do so in their male siblings (Figures 3E and 3G). Similarly, antimycin A treatment had a pronounced effect in hermaphrodites but only marginally increased p<sub>hsp-6</sub>-GFP expression in males (Figures 3F and 3H). This phenotype was specific for the UPR<sup>mt</sup>, as males were able to induce both the HSR and O<sub>2</sub>SR to a greater extent than their hermaphrodite siblings upon stress (Figures S8A–S8D). These results indicate that the UPR<sup>mt</sup> is a sexually dimorphic stress response and highlight the importance of oocytes and active reproduction per se for UPR<sup>mt</sup> induction in somatic cells.

### Non-cell-autonomous induction of UPR<sup>mt</sup> upon mitochondrial stress in the germline

We further investigated the interplay between germline and soma in the regulation of UPR<sup>mt</sup>. To this end, we used strains that allow tissue-specific RNAi-mediated knockdown. We tested *ppw-1* mutants, which are inherently RNAi deficient in the germline, allowing mitochondrial stress induction by RNAi only in the soma.<sup>54</sup> We found that *ppw-1(tm5919)* mutants could induce p<sub>hsp-6</sub>-GFP expression similarly to wild-type worms when mitochondrial stress was applied from hatching (Figures 4A–4C) or the L4 larval stage (Figures S9A and S9B), with the only exception of *cco-1* knockdown from the L4 stage. Thus, the perception of mitochondrial stress in the germline is generally not required for somatic UPR<sup>mt</sup> induction but may be supportive for specific types of mitochondrial stress.

We next asked whether mitochondrial stress in the germline could activate UPR<sup>mt</sup> in the soma. To address this question, we crossed our UPR<sup>mt</sup> reporter with a strain that allows RNAi-mediated silencing exclusively in the germline.<sup>55</sup> In contrast to the wild type, these animals were resistant to RNAi-mediated downregulation of GFP in the soma (Figures 4A and 4B) and did not exhibit the developmental defects associated with ETC inhibition (Figure 4D), highlighting the germline specificity of the RNAi-mediated silencing. Interestingly, administration of germline-specific mitochondrial stress from hatching could induce somatic p<sub>hsp-6</sub>-GFP expression, although to a lesser extent than

systemic mitochondrial stress (Figures 4A–4C and 4E). Furthermore, germline-specific knockdown of *atp-3*, the most potent UPR<sup>mt</sup> RNAi inducer from the L4 larval stage, increased somatic p<sub>hsp-6</sub>-GFP expression (Figures S9C–S9E). This non-cell-autonomous UPR<sup>mt</sup> induction is not correlated with lifespan changes, since only germline-specific knockdown of *isp-1* extended the lifespan (Figure 4F). These results demonstrate that mitochondrial stress in the germline is sufficient to induce UPR<sup>mt</sup> in the soma of *C. elegans*.

### DISCUSSION

UPR<sup>mt</sup> enables recovery from mitochondrial stress; however, its prolonged activation is detrimental to organismal homeostasis. Importantly, UPR<sup>mt</sup> activation does not always correlate with increased lifespan, and *atfs-1* gain-of-function mutants are short lived.<sup>56,57</sup> In addition, UPR<sup>mt</sup> facilitates the spread of a selfish mitochondrial genome in heteroplasmic nematode strains.<sup>58,59</sup> UPR<sup>mt</sup> activation has also been associated with cancer cell populations with increased metastatic capacity and invasiveness,<sup>60</sup> highlighting the need for tight control of the UPR<sup>mt</sup>. In the present study, we provide insight into the physiological coordination of UPR<sup>mt</sup> induction with reproduction in the multicellular organism *C. elegans*. Our results suggest that somatic UPR<sup>mt</sup> inducibility decreases with sperm depletion and fewer oocytes maturing by self-fertilization in aging hermaphroditic worms. As a proof of principle, restoring fertility by mating with sperm-producing males partially rescued the potential of feminized worms to activate the UPR<sup>mt</sup>.

The UPR<sup>mt</sup> can be activated in a non-cell-autonomous manner. Neuron-specific knockdown of ETC components, pan-neuronal expression of polyglutamine tracts that physically associate with mitochondria and compromise their fitness, or disruption of mitochondrial dynamics induces the expression of mitochondrial chaperones in the *C. elegans* intestine.<sup>22–25</sup> Several neurotransmitters (serotonin, glutamate, and acetylcholine), neuromodulators (tyramine), neuropeptides (FLP-2), and the EGL-20 ligand have been implicated in the cell non-autonomous induction of the UPR<sup>mt</sup>.<sup>24,25,61</sup> Mitochondrial stress in the germline via genetic inhibition of *cyc-2.1* also induces UPR<sup>mt</sup> non-cell-autonomously.<sup>62</sup> In *Drosophila*, mitochondrial stress in muscles enhances the production of an insulin antagonist peptide to systematically suppress insulin signaling,<sup>63</sup> and ETC complex I inhibition affects lipid metabolism in the fat body via a secreted transforming growth factor  $\beta$  (TGF- $\beta$ ) ligand.<sup>64</sup> In humans, FGF-21 secretion increases hepatic ketogenesis and

(C) Photomicrographs of day 2 adult WT and *fem-1(hc17ts)* mutant p<sub>hsp-6</sub>-GFP reporter nematodes mated with WT and *daf-22(m130)* males and treated with antimycin A.

(D) Quantification of p<sub>hsp-6</sub>-GFP fluorescence in WT and *fem-1(hc17ts)* mutants upon mating with males and subsequent antimycin A treatment ( $n = 3$ , \*\* $p < 0.01$ , two-way ANOVA).

(E) Photomicrographs of day 3 adult hermaphrodite (XX) and male (X0) p<sub>hsp-6</sub>-GFP reporter siblings treated with EV, *cco-1(RNAi)*, and *atp-3(RNAi)* from the L4 larval stage.

(F) Photomicrographs of day 2 adult hermaphrodite (XX) and male (X0) p<sub>hsp-6</sub>-GFP siblings treated with antimycin A.

(G) Quantification of p<sub>hsp-6</sub>-GFP fluorescence in day 3 adult hermaphrodites (XX) and males (X0) treated with EV and two UPR<sup>mt</sup>-inducing RNAis from the L4 larval stage ( $n > 3$ , \*\*\* $p < 0.001$ , two-way ANOVA).

(H) Quantification of p<sub>hsp-6</sub>-GFP fluorescence in WT day 2 adult hermaphrodites (XX) and males (X0) upon antimycin A treatment ( $n > 3$ , \*\*\* $p < 0.001$ , two-way ANOVA).

Data are represented as mean  $\pm$  SD. Scale bars, 200  $\mu$ m.

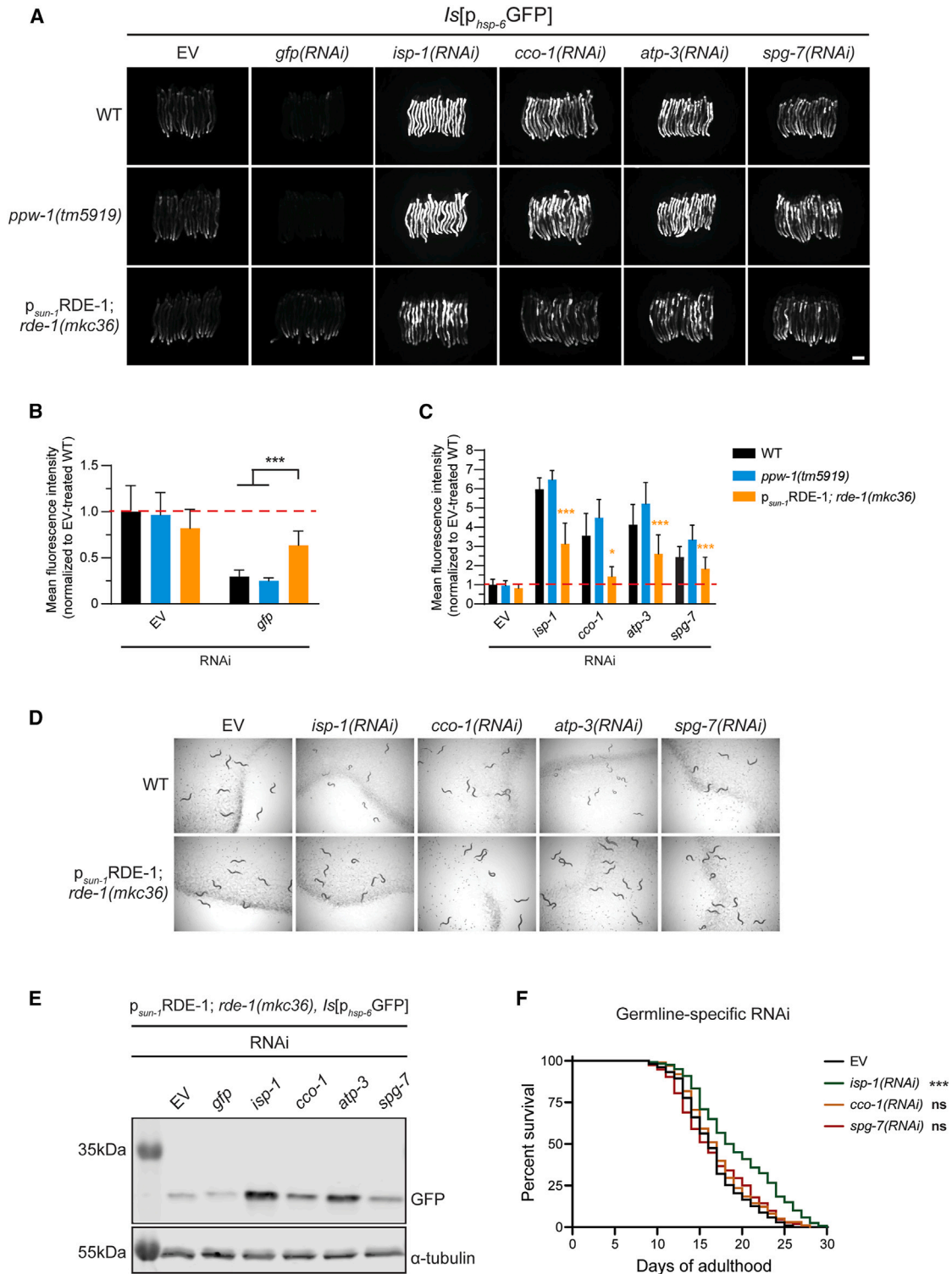


**Figure 4. Non-cell-autonomous UPR<sup>mt</sup> induction in response to germline mitochondrial stress**

(A) Photomicrographs of day 1 adult WT, *ppw-1(tm5919)*, and  $p_{sun-1}\text{RDE-1}; rde-1(mkc36)$   $p_{hsp-6}\text{GFP}$  reporter nematodes treated with EV, *gfp(RNAi)*, and four UPR<sup>mt</sup>-inducing RNAs for three consecutive days after hatching.

(B) Quantification of intestinal  $p_{hsp-6}\text{GFP}$  fluorescence in WT, *ppw-1(tm5919)*, and  $p_{sun-1}\text{RDE-1}; rde-1(mkc36)$   $p_{hsp-6}\text{GFP}$  reporter nematodes upon treatment with EV and *gfp(RNAi)* from hatching ( $n = 3$ , \*\*\* $p < 0.001$ , two-way ANOVA).

(legend continued on next page)

lipolysis in patients with mitochondrial myopathies.<sup>65</sup> In our experimental paradigm, germline-to-soma signaling largely determines the potential of adult nematodes to respond to mitochondrial stress. We show that active reproduction, rather than the perception of mitochondrial stress in the germline, is required for efficient UPR<sup>mt</sup> induction. It is reasonable to speculate that this serves as a line of defense to protect somatic mitochondria of reproductively active adults from stress. We propose that the germline maintains UPR<sup>mt</sup> inducibility in the intestine, which, in turn, supports the germline through the synthesis and secretion of egg yolk, which provides nutrients to the developing embryos.

Taken together, we suggest that reproductive signals are indispensable for the robust induction of UPR<sup>mt</sup> in somatic tissues. Consequently, somatic cells remain competent for UPR<sup>mt</sup> induction as long as the organism produces viable offspring. Our results provide evidence for a germline-to-soma signaling axis that regulates a key stress response.

### Limitations of the study

Our genetic analysis has revealed a link between germline homeostasis and somatic UPR<sup>mt</sup> inducibility. We anticipate that future studies will elucidate the identity of the germline-derived signals that maintain full UPR<sup>mt</sup> activity as long as the animals are fertile.

### STAR★METHODS

Detailed methods are provided in the online version of this paper and include the following:

- KEY RESOURCES TABLE
- RESOURCE AVAILABILITY
  - Lead contact
  - Materials availability
  - Data and code availability
- EXPERIMENTAL MODEL AND STUDY PARTICIPANT DETAILS
  - *C. elegans* strains
- METHOD DETAILS
  - Strain maintenance and genetics
  - RNAi experiments
  - Antimycin A treatment
  - ER stress induction
  - Heat stress induction
  - Oxidative stress induction
  - FUDR treatment
  - Ionizing (IR) and ultraviolet (UV-B) irradiation
  - Mating
  - Western blotting
  - BioSorter fluorescence quantification
  - Microscopy and image processing
  - Lifespan assay
- QUANTIFICATION AND STATISTICAL ANALYSIS

(C) Quantification of intestinal p<sub>hsp-6</sub>-GFP fluorescence in WT, *ppw-1(tm5919)*, and *p<sub>sun-1</sub>RDE-1; rde-1(mkc36)* p<sub>hsp-6</sub>-GFP reporter nematodes upon treatment with four UPR<sup>mt</sup>-inducing RNAis ( $n = 3$ , \*\*\* $p < 0.001$ , \* $p < 0.05$ , two-way ANOVA).

(D) Photomicrographs of day 1 adult WT and *p<sub>sun-1</sub>RDE-1; rde-1(mkc36)* nematodes treated with EV and four UPR<sup>mt</sup>-inducing RNAis for three consecutive days after hatching.

(E) Western blot of worm lysates detecting p<sub>hsp-6</sub>-GFP and  $\alpha$ -tubulin in *p<sub>sun-1</sub>RDE-1; rde-1(mkc36)* worms.

(F) Lifespan analysis of *p<sub>sun-1</sub>RDE-1; rde-1(mkc36)* worms treated with EV, *isp-1(RNAi)*, *cco-1(RNAi)*, and *spg-7(RNAi)* from hatching ( $n = 2$ , \*\*\* $p < 0.001$ , log rank [Mantel-Cox] test).

Data are represented as mean  $\pm$  SD. Scale bar, 200  $\mu$ m.

### SUPPLEMENTAL INFORMATION

Supplemental information can be found online at <https://doi.org/10.1016/j.celrep.2024.114336>.

### ACKNOWLEDGMENTS

We acknowledge E. Kyriakakis, G. Anagnostopoulos, and C. Ploumi for critically reading the manuscript. Nematode strains used in this work were provided by the Caenorhabditis Genetics Center (CGC), which is funded by NIH Office of Research Infrastructure Programs (P40 OD010440), and S. Mitani (National Bioresource Project) in Japan. We thank A. Antebi, E. Lambie, B. Schumacher, and D. Vilchez for providing worm strains and A. Franz for generating the strain PP2673. We thank A. Fire for plasmids. The graphical abstract and Figure 1G were created with BioRender. We thank all members of the Hoppe and Tavernarakis labs for helpful suggestions. This work was funded by the European Research Council (grant ERC-GA695190, acronym MANNA), the European Commission Framework Programs, and the Greek Ministry of Education (to N.T.). This work was funded by the Deutsche Forschungsgemeinschaft (DFG; German Research Foundation) under Germany's Excellence Strategy – EXC 2030 – 390661388 and – FOR 5504 – project number 496650118 (to T.H.). N.C. was supported by the project “BIOIMAGING-GR” (MIS5002755), which is implemented under the Action “Reinforcement of the Research and Innovation Infrastructure” funded by the Operational Program “Competitiveness, Entrepreneurship and Innovation” (NSRF 2014-2020), by an Alexander von Humboldt Foundation postdoctoral fellowship, and FOR 5504.

### AUTHOR CONTRIBUTIONS

N.C. conceived the study and designed experiments. N.C., A.S., and K.A. performed experiments and analyzed data. N.C. and T.H. wrote the manuscript. N.T. and T.H. supervised the experimental design and data interpretation and provided financial support.

### DECLARATION OF INTERESTS

The authors declare no competing interests.

Received: November 28, 2023

Revised: April 22, 2024

Accepted: May 23, 2024

Published: June 7, 2024

### REFERENCES

1. Lopez-Otin, C., Blasco, M.A., Partridge, L., Serrano, M., and Kroemer, G. (2013). The hallmarks of aging. *Cell* 153, 1194–1217. <https://doi.org/10.1016/j.cell.2013.05.039>.
2. Hipp, M.S., Kasturi, P., and Hartl, F.U. (2019). The proteostasis network and its decline in ageing. *Nat. Rev. Mol. Cell Biol.* 20, 421–435. <https://doi.org/10.1038/s41580-019-0101-y>.
3. Higuchi-Sanabria, R., Frankino, P.A., Paul, J.W., 3rd, Tronnes, S.U., and Dillin, A. (2018). A Futile Battle? Protein Quality Control and the Stress of Aging. *Dev. Cell* 44, 139–163. <https://doi.org/10.1016/j.devcel.2017.12.020>.

4. Ben-Zvi, A., Miller, E.A., and Morimoto, R.I. (2009). Collapse of proteostasis represents an early molecular event in *Caenorhabditis elegans* aging. *Proc. Natl. Acad. Sci. USA* *106*, 14914–14919. <https://doi.org/10.1073/pnas.0902882106>.
5. David, D.C., Ollikainen, N., Trinidad, J.C., Cary, M.P., Burlingame, A.L., and Kenyon, C. (2010). Widespread protein aggregation as an inherent part of aging in *C. elegans*. *PLoS Biol.* *8*, e1000450. <https://doi.org/10.1371/journal.pbio.1000450>.
6. Rolland, S.G., Schneid, S., Schwarz, M., Rackles, E., Fischer, C., Haeussler, S., Regmi, S.G., Yeroslaviz, A., Habermann, B., Mokranjac, D., et al. (2019). Compromised Mitochondrial Protein Import Acts as a Signal for UPR(mt). *Cell Rep.* *28*, 1659–1669.e5. <https://doi.org/10.1016/j.celrep.2019.07.049>.
7. Houtkooper, R.H., Mouchiroud, L., Ryu, D., Moullan, N., Katsyuba, E., Knott, G., Williams, R.W., and Auwerx, J. (2013). Mitonuclear protein imbalance as a conserved longevity mechanism. *Nature* *497*, 451–457. <https://doi.org/10.1038/nature12188>.
8. Shpilka, T., and Haynes, C.M. (2018). The mitochondrial UPR: mechanisms, physiological functions and implications in ageing. *Nat. Rev. Mol. Cell Biol.* *19*, 109–120. <https://doi.org/10.1038/nrm.2017.110>.
9. Nargund, A.M., Pellegrino, M.W., Fiorese, C.J., Baker, B.M., and Haynes, C.M. (2012). Mitochondrial import efficiency of ATFS-1 regulates mitochondrial UPR activation. *Science* *337*, 587–590. <https://doi.org/10.1126/science.1223560>.
10. Nargund, A.M., Fiorese, C.J., Pellegrino, M.W., Deng, P., and Haynes, C.M. (2015). Mitochondrial and nuclear accumulation of the transcription factor ATFS-1 promotes OXPHOS recovery during the UPR(mt). *Mol. Cell* *58*, 123–133. <https://doi.org/10.1016/j.molcel.2015.02.008>.
11. Pellegrino, M.W., Nargund, A.M., Kirienko, N.V., Gillis, R., Fiorese, C.J., and Haynes, C.M. (2014). Mitochondrial UPR-regulated innate immunity provides resistance to pathogen infection. *Nature* *516*, 414–417. <https://doi.org/10.1038/nature13818>.
12. Benedetti, C., Haynes, C.M., Yang, Y., Harding, H.P., and Ron, D. (2006). Ubiquitin-like protein 5 positively regulates chaperone gene expression in the mitochondrial unfolded protein response. *Genetics* *174*, 229–239. <https://doi.org/10.1534/genetics.106.061580>.
13. Tian, Y., Garcia, G., Bian, Q., Steffen, K.K., Joe, L., Wolff, S., Meyer, B.J., and Dillin, A. (2016). Mitochondrial Stress Induces Chromatin Reorganization to Promote Longevity and UPR(mt). *Cell* *165*, 1197–1208. <https://doi.org/10.1016/j.cell.2016.04.011>.
14. Merkwirth, C., Jovaisaite, V., Durieux, J., Matilainen, O., Jordan, S.D., Quiros, P.M., Steffen, K.K., Williams, E.G., Mouchiroud, L., Tronnes, S.U., et al. (2016). Two Conserved Histone Demethylases Regulate Mitochondrial Stress-Induced Longevity. *Cell* *165*, 1209–1223. <https://doi.org/10.1016/j.cell.2016.04.012>.
15. Haynes, C.M., Petrova, K., Benedetti, C., Yang, Y., and Ron, D. (2007). ClpP mediates activation of a mitochondrial unfolded protein response in *C. elegans*. *Dev. Cell* *13*, 467–480. <https://doi.org/10.1016/j.devcel.2007.07.016>.
16. Li, T.Y., Sleiman, M.B., Li, H., Gao, A.W., Mottis, A., Bachmann, A.M., El Alam, G., Li, X., Goeminne, L.J.E., Schoonjans, K., and Auwerx, J. (2021). The transcriptional coactivator CBP/p300 is an evolutionarily conserved node that promotes longevity in response to mitochondrial stress. *Nat. Aging* *1*, 165–178. <https://doi.org/10.1038/s43587-020-00025-z>.
17. Kim, S., and Sieburth, D. (2018). Sphingosine Kinase Activates the Mitochondrial Unfolded Protein Response and Is Targeted to Mitochondria by Stress. *Cell Rep.* *24*, 2932–2945.e4. <https://doi.org/10.1016/j.celrep.2018.08.037>.
18. Shao, L.W., Peng, Q., Dong, M., Gao, K., Li, Y., Li, Y., Li, C.Y., and Liu, Y. (2020). Histone deacetylase HDA-1 modulates mitochondrial stress response and longevity. *Nat. Commun.* *11*, 4639. <https://doi.org/10.1038/s41467-020-18501-w>.
19. Zhao, Q., Wang, J., Levichkin, I.V., Stasinopoulos, S., Ryan, M.T., and Hoogenraad, N.J. (2002). A mitochondrial specific stress response in mammalian cells. *EMBO J.* *21*, 4411–4419. <https://doi.org/10.1093/emboj/cdf445>.
20. Fiorese, C.J., Schulz, A.M., Lin, Y.F., Rosin, N., Pellegrino, M.W., and Haynes, C.M. (2016). The Transcription Factor ATF5 Mediates a Mammalian Mitochondrial UPR. *Curr. Biol.* *26*, 2037–2043. <https://doi.org/10.1016/j.cub.2016.06.002>.
21. Quiros, P.M., Prado, M.A., Zamboni, N., D’Amico, D., Williams, R.W., Finley, D., Gygi, S.P., and Auwerx, J. (2017). Multi-omics analysis identifies ATF4 as a key regulator of the mitochondrial stress response in mammals. *J. Cell Biol.* *216*, 2027–2045. <https://doi.org/10.1083/jcb.201702058>.
22. Durieux, J., Wolff, S., and Dillin, A. (2011). The cell-non-autonomous nature of electron transport chain-mediated longevity. *Cell* *144*, 79–91. <https://doi.org/10.1016/j.cell.2010.12.016>.
23. Berendzen, K.M., Durieux, J., Shao, L.W., Tian, Y., Kim, H.E., Wolff, S., Liu, Y., and Dillin, A. (2016). Neuroendocrine Coordination of Mitochondrial Stress Signaling and Proteostasis. *Cell* *166*, 1553–1563.e10. <https://doi.org/10.1016/j.cell.2016.08.042>.
24. Shao, L.W., Niu, R., and Liu, Y. (2016). Neuropeptide signals cell non-autonomous mitochondrial unfolded protein response. *Cell Res.* *26*, 1182–1196. <https://doi.org/10.1038/cr.2016.118>.
25. Chen, L.T., Lin, C.T., Lin, L.Y., Hsu, J.M., Wu, Y.C., and Pan, C.L. (2021). Neuronal mitochondrial dynamics coordinate systemic mitochondrial morphology and stress response to confer pathogen resistance in *C. elegans*. *Dev. Cell* *56*, 1770–1785.e12. <https://doi.org/10.1016/j.devcel.2021.04.021>.
26. Charmpilas, N., and Tavernarakis, N. (2020). Mitochondrial maturation drives germline stem cell differentiation in *Caenorhabditis elegans*. *Cell Death Differ.* *27*, 601–617. <https://doi.org/10.1038/s41418-019-0375-9>.
27. Arantes-Oliveira, N., Apfeld, J., Dillin, A., and Kenyon, C. (2002). Regulation of Life-Span by Germ-Line Stem Cells in *Caenorhabditis elegans*. *Science* *295*, 502–505. <https://doi.org/10.1126/science.1065768>.
28. Kimble, J., and Crittenden, S.L. (2005). Germline proliferation and its control. *WormBook.*, 1–14. <https://doi.org/10.1895/wormbook.1.13.1>.
29. Austin, J., and Kimble, J. (1987). *glp-1* is required in the germ line for regulation of the decision between mitosis and meiosis in *C. elegans*. *Cell* *51*, 589–599. [https://doi.org/10.1016/0092-8674\(87\)90128-0](https://doi.org/10.1016/0092-8674(87)90128-0).
30. Yoneda, T., Benedetti, C., Urano, F., Clark, S.G., Harding, H.P., and Ron, D. (2004). Compartment-specific perturbation of protein handling activates genes encoding mitochondrial chaperones. *J. Cell Sci.* *117*, 4055–4066. <https://doi.org/10.1242/jcs.01275>.
31. Angeli, S., Foulger, A., Chamoli, M., Peiris, T.H., Gerencser, A., Shahmirzadi, A.A., Andersen, J., and Lithgow, G. (2021). The mitochondrial permeability transition pore activates the mitochondrial unfolded protein response and promotes aging. *Elife* *10*, e63453. <https://doi.org/10.7554/eLife.63453>.
32. Labbadia, J., Briellmann, R.M., Neto, M.F., Lin, Y.F., Haynes, C.M., and Morimoto, R.I. (2017). Mitochondrial Stress Restores the Heat Shock Response and Prevents Proteostasis Collapse during Aging. *Cell Rep.* *21*, 1481–1494. <https://doi.org/10.1016/j.celrep.2017.10.038>.
33. Liu, Y., Samuel, B.S., Breen, P.C., and Ruvkun, G. (2014). *Caenorhabditis elegans* pathways that surveil and defend mitochondria. *Nature* *508*, 406–410. <https://doi.org/10.1038/nature13204>.
34. Berman, J.R., and Kenyon, C. (2006). Germ-cell loss extends *C. elegans* life span through regulation of DAF-16 by *kri-1* and lipophilic-hormone signaling. *Cell* *124*, 1055–1068. <https://doi.org/10.1016/j.cell.2006.01.039>.
35. Beanan, M.J., and Strome, S. (1992). Characterization of a germ-line proliferation mutation in *C. elegans*. *Development* *116*, 755–766.
36. Rastogi, S., Borgo, B., Pazdernik, N., Fox, P., Mardis, E.R., Kohara, Y., Havranek, J., and Schedl, T. (2015). *Caenorhabditis elegans glp-4*

- Encodes a Valyl Aminoacyl tRNA Synthetase. *G3* (Bethesda). 5, 2719–2728. <https://doi.org/10.1534/g3.115.021899>.
37. Frakes, A.E., and Dillin, A. (2017). The UPR(ER): Sensor and Coordinator of Organismal Homeostasis. *Mol. Cell* 66, 761–771. <https://doi.org/10.1016/j.molcel.2017.05.031>.
  38. Taylor, R.C., and Dillin, A. (2013). XBP-1 is a cell-nonautonomous regulator of stress resistance and longevity. *Cell* 153, 1435–1447. <https://doi.org/10.1016/j.cell.2013.05.042>.
  39. Pepper, A.S.R., Lo, T.W., Killian, D.J., Hall, D.H., and Hubbard, E.J.A. (2003). The establishment of *Caenorhabditis elegans* germline pattern is controlled by overlapping proximal and distal somatic gonad signals. *Dev. Biol.* 259, 336–350. [https://doi.org/10.1016/s0012-1606\(03\)00203-3](https://doi.org/10.1016/s0012-1606(03)00203-3).
  40. Tsang, W.Y., and Lemire, B.D. (2002). Mitochondrial Genome Content Is Regulated during Nematode Development. *Biochem. Biophys. Res. Commun.* 297, 8–16. <https://doi.org/10.1006/bbrc.2002.6394>.
  41. Bratic, I., Hench, J., Henriksson, J., Antebi, A., Bürglin, T.R., and Trifunovic, A. (2009). Mitochondrial DNA level, but not active replicase, is essential for *Caenorhabditis elegans* development. *Nucleic Acids Res.* 37, 1817–1828. <https://doi.org/10.1093/nar/gkp018>.
  42. Sulston, J.E., Schierenberg, E., White, J.G., and Thomson, J.N. (1983). The embryonic cell lineage of the nematode *Caenorhabditis elegans*. *Dev. Biol.* 100, 64–119. [https://doi.org/10.1016/0012-1606\(83\)90201-4](https://doi.org/10.1016/0012-1606(83)90201-4).
  43. Berkowitz, L.A., and Strome, S. (2000). MES-1, a protein required for unequal divisions of the germline in early *C. elegans* embryos, resembles receptor tyrosine kinases and is localized to the boundary between the germline and gut cells. *Development* 127, 4419–4431.
  44. Sun, A.Y., and Lambie, E.J. (1997). *gon-2*, a gene required for gonadogenesis in *Caenorhabditis elegans*. *Genetics* 147, 1077–1089.
  45. Ackermann, L., Schell, M., Pokrzywa, W., Kevei, É., Gartner, A., Schumacher, B., and Hoppe, T. (2016). E4 ligase-specific ubiquitination hubs coordinate DNA double-strand-break repair and apoptosis. *Nat. Struct. Mol. Biol.* 23, 995–1002. <https://doi.org/10.1038/nsmb.3296>.
  46. Ermolaeva, M.A., Segref, A., Dakhovnik, A., Ou, H.L., Schneider, J.I., Utermöhlen, O., Hoppe, T., and Schumacher, B. (2013). DNA damage in germ cells induces an innate immune response that triggers systemic stress resistance. *Nature* 501, 416–420. <https://doi.org/10.1038/nature12452>.
  47. Hodgkin, J. (1986). Sex determination in the nematode *C. elegans*: analysis of *tra-3* suppressors and characterization of *fem* genes. *Genetics* 114, 15–52.
  48. Maures, T.J., Booth, L.N., Benayoun, B.A., Izrayelit, Y., Schroeder, F.C., and Brunet, A. (2014). Males shorten the life span of *C. elegans* hermaphrodites via secreted compounds. *Science* 343, 541–544. <https://doi.org/10.1126/science.1244160>.
  49. Gomez-Pastor, R., Burchfiel, E.T., and Thiele, D.J. (2018). Regulation of heat shock transcription factors and their roles in physiology and disease. *Nat. Rev. Mol. Cell Biol.* 19, 4–19. <https://doi.org/10.1038/nrm.2017.73>.
  50. Das, R., Melo, J.A., Thondamal, M., Morton, E.A., Cornwell, A.B., Crick, B., Kim, J.H., Swartz, E.W., Lamitina, T., Douglas, P.M., and Samuelson, A.V. (2017). The homeodomain-interacting protein kinase HPK-1 preserves protein homeostasis and longevity through master regulatory control of the HSF-1 chaperone network and TORC1-restricted autophagy in *Caenorhabditis elegans*. *PLoS Genet.* 13, e1007038. <https://doi.org/10.1371/journal.pgen.1007038>.
  51. Brunquell, J., Morris, S., Lu, Y., Cheng, F., and Westerheide, S.D. (2016). The genome-wide role of HSF-1 in the regulation of gene expression in *Caenorhabditis elegans*. *BMC Genom.* 17, 559. <https://doi.org/10.1186/s12864-016-2837-5>.
  52. Blackwell, T.K., Steinbaugh, M.J., Hourihan, J.M., Ewald, C.Y., and Isik, M. (2015). SKN-1/Nrf, stress responses, and aging in *Caenorhabditis elegans*. *Free Radic. Biol. Med.* 88, 290–301. <https://doi.org/10.1016/j.freeradbiomed.2015.06.008>.
  53. Hu, Q., D'Amora, D.R., MacNeil, L.T., Walhout, A.J.M., and Kubiseski, T.J. (2018). The *Caenorhabditis elegans* Oxidative Stress Response Requires the NHR-49 Transcription Factor. *G3* (Bethesda, Md.) 8, 3857–3863. <https://doi.org/10.1534/g3.118.200727>.
  54. Tijsterman, M., Okihara, K.L., Thijssen, K., and Plasterk, R.H.A. (2002). PPW-1, a PAZ/PIWI protein required for efficient germline RNAi, is defective in a natural isolate of *C. elegans*. *Curr. Biol.* 12, 1535–1540. [https://doi.org/10.1016/s0960-9822\(02\)01110-7](https://doi.org/10.1016/s0960-9822(02)01110-7).
  55. Zou, L., Wu, D., Zang, X., Wang, Z., Wu, Z., and Chen, D. (2019). Construction of a germline-specific RNAi tool in *C. elegans*. *Sci. Rep.* 9, 2354. <https://doi.org/10.1038/s41598-019-38950-8>.
  56. Bennett, C.F., Vander Wende, H., Simko, M., Klum, S., Barfield, S., Choi, H., Pineda, V.V., and Kaerberlein, M. (2014). Activation of the mitochondrial unfolded protein response does not predict longevity in *Caenorhabditis elegans*. *Nat. Commun.* 5, 3483. <https://doi.org/10.1038/ncomms4483>.
  57. Rauthan, M., Ranji, P., Aguilera Pradenas, N., Pitot, C., and Pilon, M. (2013). The mitochondrial unfolded protein response activator ATFS-1 protects cells from inhibition of the mevalonate pathway. *Proc. Natl. Acad. Sci. USA* 110, 5981–5986. <https://doi.org/10.1073/pnas.1218778110>.
  58. Lin, Y.F., Schulz, A.M., Pellegrino, M.W., Lu, Y., Shaham, S., and Haynes, C.M. (2016). Maintenance and propagation of a deleterious mitochondrial genome by the mitochondrial unfolded protein response. *Nature* 533, 416–419. <https://doi.org/10.1038/nature17989>.
  59. Gitschlag, B.L., Kirby, C.S., Samuels, D.C., Gangula, R.D., Mallal, S.A., and Patel, M.R. (2016). Homeostatic Responses Regulate Selfish Mitochondrial Genome Dynamics in *C. elegans*. *Cell Metab.* 24, 91–103. <https://doi.org/10.1016/j.cmet.2016.06.008>.
  60. Kenny, T.C., Craig, A.J., Villanueva, A., and Germain, D. (2019). Mitohormesis Primes Tumor Invasion and Metastasis. *Cell Rep.* 27, 2292–2303.e6. <https://doi.org/10.1016/j.celrep.2019.04.095>.
  61. Zhang, Q., Wu, X., Chen, P., Liu, L., Xin, N., Tian, Y., and Dillin, A. (2018). The Mitochondrial Unfolded Protein Response Is Mediated Cell-Non-autonomously by Retromer-Dependent Wnt Signaling. *Cell* 174, 870–883.e17. <https://doi.org/10.1016/j.cell.2018.06.029>.
  62. Lan, J., Rollins, J.A., Zang, X., Wu, D., Zou, L., Wang, Z., Ye, C., Wu, Z., Kapahi, P., Rogers, A.N., and Chen, D. (2019). Translational Regulation of Non-autonomous Mitochondrial Stress Response Promotes Longevity. *Cell Rep.* 28, 1050–1062.e6. <https://doi.org/10.1016/j.celrep.2019.06.078>.
  63. Owusu-Ansah, E., Song, W., and Perrimon, N. (2013). Muscle mitohormesis promotes longevity via systemic repression of insulin signaling. *Cell* 155, 699–712. <https://doi.org/10.1016/j.cell.2013.09.021>.
  64. Song, W., Owusu-Ansah, E., Hu, Y., Cheng, D., Ni, X., Zirin, J., and Perrimon, N. (2017). Activin signaling mediates muscle-to-adipose communication in a mitochondria dysfunction-associated obesity model. *Proc. Natl. Acad. Sci. USA* 114, 8596–8601. <https://doi.org/10.1073/pnas.1708037114>.
  65. Suomalainen, A., Elo, J.M., Pietiläinen, K.H., Hakonen, A.H., Sevastianova, K., Korpela, M., Isohanni, P., Marjavaara, S.K., Tyni, T., Kiuru-Enari, S., et al. (2011). FGF-21 as a biomarker for muscle-manifesting mitochondrial respiratory chain deficiencies: a diagnostic study. *Lancet Neurol.* 10, 806–818. [https://doi.org/10.1016/S1474-4422\(11\)70155-7](https://doi.org/10.1016/S1474-4422(11)70155-7).
  66. Brenner, S. (1974). The genetics of *Caenorhabditis elegans*. *Genetics* 77, 71–94.
  67. Rual, J.F., Ceron, J., Koreth, J., Hao, T., Nicot, A.S., Hirozane-Kishikawa, T., Vandenhaute, J., Orkin, S.H., Hill, D.E., van den Heuvel, S., and Vidal, M. (2004). Toward improving *Caenorhabditis elegans* phenotype mapping with an ORFeome-based RNAi library. *Genome Res.* 14, 2162–2168. <https://doi.org/10.1101/gr.2505604>.

## STAR★METHODS

### KEY RESOURCES TABLE

REAGENT or RESOURCE	SOURCE	IDENTIFIER
<b>Antibodies</b>		
Anti-living colors monoclonal antibody (JL-8)	Takara Bio	Cat# 632380; RRID:AB_10013427
Anti-alpha tubulin mouse monoclonal, clone B-5-1-2	Sigma-Aldrich	Cat# T5168; RRID:AB_477579
Donkey Anti-Mouse IgG IRDye 680 Conjugated secondary	LI-COR Biosciences	Cat# 926-32222; RRID:AB_621844
Donkey anti-Mouse IgG IRDye 800CWsecondary	LI-COR Biosciences	Cat# 926-32212; RRID:AB_621847
<b>Bacterial and virus strains</b>		
<i>E. coli</i> : OP50	CGC	OP50
<i>E. coli</i> : HT115 cells transformed with an empty pL4440 vector construct	Home-made	EV
<i>E. coli</i> : HT115 cells transformed with a pL4440- <i>isp-1</i> (RNAi) construct	Home-made	<i>isp-1</i> (RNAi)
<i>E. coli</i> : HT115 cells transformed with a pL4440- <i>cco-1</i> (RNAi) construct	ORFeome RNAi library	<i>cco-1</i> (RNAi)
<i>E. coli</i> : HT115 cells transformed with a pL4440- <i>atp-3</i> (RNAi) construct	ORFeome RNAi library	<i>atp-3</i> (RNAi)
<i>E. coli</i> : HT115 cells transformed with a pL4440- <i>spg-7</i> (RNAi) construct	ORFeome RNAi library	<i>spg-7</i> (RNAi)
<i>E. coli</i> : HT115 cells transformed with a pL4440- <i>ero-1</i> (RNAi) construct	ORFeome RNAi library	<i>ero-1</i> (RNAi)
<i>E. coli</i> : HT115 cells transformed with a pL4440- <i>polg-1</i> (RNAi) construct	Home-made	<i>polg-1</i> (RNAi)
<i>E. coli</i> : HT115 cells transformed with a pL4440- <i>gfp</i> (RNAi) construct	Home-made	<i>gfp</i> (RNAi)
<b>Chemicals, peptides, and recombinant proteins</b>		
Antimycin A (CAS number: 1397-94-0)	Sigma-Aldrich	A8674
Tunicamycin (CAS number: 11089-65-9)	Sigma-Aldrich	T7765
Paraquat (methyl viologen dichloride, CAS number: 75365-73-0)	Sigma-Aldrich	856177
5-fluoro-2'-deoxyuridine (FUDR, CAS number: 50-91-9)	Sigma-Aldrich	F0503
Tetramisole hydrochloride (CAS number: 16595-80-5)	Sigma-Aldrich	L9756
<b>Critical commercial assays</b>		
OneTaq® 2X Master Mix	New England Biolabs	Cat# M0482S
<b>Experimental models: Organisms/strains</b>		
<i>C. elegans</i> strain PP1: N2 (WT)	CGC	N2 (WT)
<i>C. elegans</i> strain PP3770: <i>daf-22(m130)</i> II	CGC	DR476
<i>C. elegans</i> strain PP923: <i>zcls13</i> [ <i>hsp-6p::GFP</i> ] V	CGC	SJ4100
<i>C. elegans</i> strain PP135: <i>zcls4</i> [ <i>hsp-4p::GFP</i> ] V	CGC	SJ4005
<i>C. elegans</i> strain PP675: <i>gpls1</i> [ <i>hsp-16.2p::GFP</i> ]	CGC	TJ375
<i>C. elegans</i> strain PP712: <i>dvls70</i> [ <i>hsp-16.2p::GFP</i> + <i>rol-6(su1006)</i> ]	CGC	CL2070
<i>C. elegans</i> strain PP1726: <i>rmls110</i> [ <i>rgef-1p::Q40:YFP</i> ]	CGC	AM101
<i>C. elegans</i> strain PP3662: <i>mkcSi13</i> [ <i>sun-1p::rde-1::sun-1 3'UTR</i> + <i>unc-119(+)</i> ] II; <i>rde-1(mkc36)</i> V	CGC	DCL569
<i>C. elegans</i> strain PP3643: <i>gfp-1(e2141ts)</i> III; <i>zcls13</i> [ <i>hsp-6p::GFP</i> ] V	This paper	N/A
<i>C. elegans</i> strain PP3678: <i>gfp-1(e2144ts)</i> III; <i>zcls13</i> [ <i>hsp-6p::GFP</i> ] V	This paper	N/A

(Continued on next page)

Continued

REAGENT or RESOURCE	SOURCE	IDENTIFIER
<i>C. elegans</i> strain PP2673: <i>atfs-1(tm4525)</i> , <i>zcls13</i> [ <i>hsp-6p::GFP</i> ] V	This paper	N/A
<i>C. elegans</i> strain PP2017: <i>glp-4(bn2ts)</i> I; <i>zcls13</i> [ <i>hsp-6p::GFP</i> ] V	This paper	N/A
<i>C. elegans</i> strain PP3815: <i>glp-1(ar202ts)</i> III; <i>zcls13</i> [ <i>hsp-6p::GFP</i> ] V	This paper	N/A
<i>C. elegans</i> strain PP3796: <i>zcls13</i> [ <i>hsp-6p::GFP</i> ] V; <i>mes-1(bn7ts)</i> X	This paper	N/A
<i>C. elegans</i> strain PP3816: <i>gon-2(q388ts)</i> I, <i>zcls13</i> [ <i>hsp-6p::GFP</i> ] V	This paper	N/A
<i>C. elegans</i> strain PP3733: <i>fem-1(hc17ts)</i> IV; <i>zcls13</i> [ <i>hsp-6p::GFP</i> ] V	This paper	N/A
<i>C. elegans</i> strain PP3805: <i>fem-3(q20ts)</i> IV; <i>zcls13</i> [ <i>hsp-6p::GFP</i> ] V	This paper	N/A
<i>C. elegans</i> strain PP3780: <i>ppw-1(tm5919)</i> I; <i>zcls13</i> [ <i>hsp-6p::GFP</i> ] V	This paper	N/A
<i>C. elegans</i> strain PP3824: <i>mkcSi13</i> [ <i>sun-1p::rde-1::sun-1 3' UTR + unc-119(+)</i> ] II; <i>rde-1(mkc36)</i> , <i>zcls13</i> [ <i>hsp-6p::GFP</i> ] V	This paper	N/A
<i>C. elegans</i> strain PP4155: <i>daf-16(mu86)</i> I; <i>glp-1(e2141ts)</i> III; <i>zcls13</i> [ <i>hsp-6p::GFP</i> ] V	This paper	N/A
<i>C. elegans</i> strain PP3656: <i>glp-1(e2141ts)</i> III; <i>zcls4</i> [ <i>hsp-4p::GFP</i> ] V	This paper	N/A
<i>C. elegans</i> strain PP3823: <i>fem-1(hc17ts)</i> IV; <i>zcls4</i> [ <i>hsp-4p::GFP</i> ] V	This paper	N/A
<i>C. elegans</i> strain PP3848: <i>fem-3(q20ts)</i> IV; <i>zcls4</i> [ <i>hsp-4p::GFP</i> ] V	This paper	N/A
<i>C. elegans</i> strain PP2626: <i>fem-1(hc17ts)</i> IV; <i>dvlS70</i> [ <i>hsp-16.2p::GFP + rol-6(su1006)</i> ]	This paper	N/A
<i>C. elegans</i> strain PP3773: <i>fem-3(q20ts)</i> IV; <i>dvlS70</i> [ <i>hsp-16.2p::GFP + rol-6(su1006)</i> ]	This paper	N/A
<i>C. elegans</i> strain PP3820: <i>dvlS19</i> [ <i>gst-4p::GFP::NLS</i> ] III; <i>fem-1(hc17ts)</i> IV	This paper	N/A
<i>C. elegans</i> strain PP3819: <i>dvlS19</i> [ <i>gst-4p::GFP::NLS</i> ] III; <i>fem-3(q20ts)</i> IV	This paper	N/A
<i>C. elegans</i> strain PP4131: <i>glp-1(e2141ts)</i> III; <i>mIs110</i> [ <i>rgef-1p::Q40:YFP</i> ]	This paper	N/A
<b>Oligonucleotides</b>		
Primer TH5511: 5'-CAGCCACAAAGTGATGAA-3' for genotyping the <i>rde-1(mkc36)</i> mutation	This paper	N/A
Primer TH5512: 5'-CTTCCTTTGTGATTTTCACTTC-3' for genotyping the <i>rde-1(mkc36)</i> mutation	This paper	N/A
Primer TH5513: 5'-CTGCTAGATGTCGAAAACCC-3' for genotyping the <i>sun-1p::rde-1::sun-1 3' UTR</i> transgene	This paper	N/A
Primer TH5514: 5'-GCAGGAACAATAATACGGCG-3' for genotyping the <i>sun-1p::rde-1::sun-1 3' UTR</i> transgene	This paper	N/A
Primer TH5515: 5'-CACTTTCCTTCATTCTCACCG-3' for genotyping the <i>ppw-1(tm5519)</i> mutation	This paper	N/A
Primer TH5516: 5'-GTCCCTTCAGCGTATTCCTTGAC-3' for genotyping the <i>ppw-1(tm5519)</i> mutation	This paper	N/A
Primer TH5660: 5'-CAAAGATTTTCCACATTCG-3' for genotyping the <i>daf-16(mu86)</i> mutation	This paper	N/A

(Continued on next page)

**Continued**

REAGENT or RESOURCE	SOURCE	IDENTIFIER
Primer TH5661: 5'-ATCAATGCTCTCTCCTTTATCC-3' for genotyping the <i>daf-16(mu86)</i> mutation	This paper	N/A
Primer TH5662: 5'-ACATAGAAGAACCAACCAACC-3' for genotyping the <i>daf-16(mu86)</i> mutation	This paper	N/A
Primer TH5663: 5'-GAAATTCAGTGCCAACAAAAG-3' for genotyping the <i>daf-16(mu86)</i> mutation	This paper	N/A

**Software and algorithms**

ZEISS ZEN software	Zeiss	Zen 2.3 lite
ImageJ/Fiji software		N/A
Graphpad Prism 8.0 software	Graphpad	<a href="https://www.graphpad.com/">https://www.graphpad.com/</a>
Adobe Illustrator 2020 software	Adobe	N/A
Snapgene Viewer software	Snapgene	<a href="https://www.snapgene.com/">https://www.snapgene.com/</a>

**Other**

BioSorter large particle flow cytometer	Union Biometrica	N/A
ZEISS Axio Zoom.V16 stereomicroscope equipped with Axiocam 506mono	Zeiss	N/A
120-kV X-rays (25 mA; 0.5mm Alu-filter; ISOVOLT 160 M1/10–55)	GE Sensing & Inspection Technologies	N/A
UV 181 BL irradiation device	Waldmann	N/A

**RESOURCE AVAILABILITY**

**Lead contact**

Further information and requests for resources and reagents should be directed to and will be fulfilled by the lead contact, Thorsten Hoppe ([thorsten.hoppe@uni-koeln.de](mailto:thorsten.hoppe@uni-koeln.de)).

**Materials availability**

All unique/stable reagents generated in this study are available from the [lead contact](#) without restriction.

**Data and code availability**

- All data reported in this paper will be shared by the [lead contact](#) upon request.
- This paper does not report original code.
- Any additional information required to reanalyze the data reported in this paper is available from the [lead contact](#) upon request.

**EXPERIMENTAL MODEL AND STUDY PARTICIPANT DETAILS**

**C. elegans strains**

The nematode strains wild-type (N2), DR476: *daf-22(m130)* II, SJ4100: *zcls13 [hsp-6p::GFP]* V, SJ4005: *zcls4 [hsp-4p::GFP]* V, TJ375: *gpls1 [hsp-16.2p::GFP]*, CL2070: *dvls70 [hsp-16.2p::GFP + rol-6(su1006)]*, CL2166: *dvls19 [gst-4p::GFP::NLS]* III, AM101: *rmls110 [rgef-1p::Q40:YFP]* and DCL569: *mkcSi13 [sun-1p::rde-1::sun-1 3'UTR + unc-119(+)]* II; *rde-1(mkc36)* V were provided by the Caenorhabditis Genetics Center (CGC), University of Minnesota, USA. The following parental mutant strains used for crosses were also acquired from CGC: CB4037: *glp-1(e2141ts)* III, CF1903: *glp-1(e2144ts)* III, SS104: *glp-4(bn2ts)* I, GC833: *glp-1(ar202ts)* III, SS149: *mes-1(bn7ts)* X, EJ1158: *gon-2(q388ts)* I, BA17: *fem-1(hc17ts)* IV, JK816: *fem-3(q20ts)* IV, CF1038: *daf-16(mu86)* I. The deletion mutants *atfs-1(tm4525)* V and *ppw-1(tm5919)* I were provided by the National Bioresource Project, Japan.

The following strains were generated in the present study: PP3643: *glp-1(e2141ts)* III; *zcls13 [hsp-6p::GFP]* V, PP3678: *glp-1(e2144ts)* III; *zcls13 [hsp-6p::GFP]* V, PP2673: *atfs-1(tm4525)*, *zcls13 [hsp-6p::GFP]* V, PP2017: *glp-4(bn2ts)* I; *zcls13 [hsp-6p::GFP]* V, PP3815: *glp-1(ar202ts)* III; *zcls13 [hsp-6p::GFP]* V, PP3796: *zcls13 [hsp-6p::GFP]* V; *mes-1(bn7ts)* X, PP3816: *gon-2(q388ts)* I, *zcls13 [hsp-6p::GFP]* V, PP3733: *fem-1(hc17ts)* IV; *zcls13 [hsp-6p::GFP]* V, PP3805: *fem-3(q20ts)* IV; *zcls13 [hsp-6p::GFP]* V, PP3780: *ppw-1(tm5919)* I; *zcls13 [hsp-6p::GFP]* V, PP3824: *mkcSi13 [sun-1p::rde-1::sun-1 3'UTR + unc-119(+)]* II; *rde-1(mkc36)*, *zcls13 [hsp-6p::GFP]* V, PP4155: *daf-16(mu86)* I; *glp-1(e2141ts)* III; *zcls13 [hsp-6p::GFP]* V, PP3656: *glp-1(e2141ts)* III; *zcls4 [hsp-4p::GFP]* V, PP3823: *fem-1(hc17ts)* IV; *zcls4 [hsp-4p::GFP]* V, PP3848: *fem-3(q20ts)* IV; *zcls4 [hsp-4p::GFP]* V, PP2626: *fem-1(hc17ts)* IV; *dvls70 [hsp-16.2p::GFP + rol-6(su1006)]*, PP3773: *fem-3(q20ts)* IV; *dvls70*

[*hsp-16.2p::GFP + rol-6(su1006)*], PP3820: *dvls19 [gst-4p::GFP::NLS]* III; *fem-1(hc17ts)* IV, PP3819: *dvls19 [gst-4p::GFP::NLS]* III; *fem-3(q20ts)* IV, PP4131: *glp-1(e2141ts)* III; *rmls110 [rgef-1p::Q40:YFP]*.

## METHOD DETAILS

### Strain maintenance and genetics

We followed standard procedures for maintaining *C. elegans* strains.<sup>66</sup> We cultured temperature-sensitive (ts) mutants strictly at the permissive temperature (15°C) side by side with their wild-type counterparts. Unless noted otherwise, a large number of wild-type and mutant eggs were synchronized at the egg stage upon hypochlorite treatment (10% 5N NaOH, 10% sodium hypochlorite solution diluted in ddH<sub>2</sub>O) and larvae that hatched were grown at the restrictive temperature (25°C) for 44 h until they reached the L4 stage. Then both wild-type and ts mutant worms were transferred at the standard rearing temperature of 20°C for the rest of the experiment. Genetic crosses with ts mutants were performed at 15°C.

### RNAi experiments

Clones encoding the genes of interest were either homemade or taken from the *C. elegans* ORF-RNAi Resource (Vidal),<sup>67</sup> distributed by Source BioScience. We confirmed that all the RNAi clones contain the right fragment by sequencing (Eurofins Genomics). For each experiment, the time point when the RNAi treatment was initiated is indicated in the text and/or the corresponding figure legends. Bacteria carrying an empty vector (EV) were used as a control treatment. Overnight cultures of HT115 *E. coli* bacteria in LB medium with 100 μg mL<sup>-1</sup> ampicillin and 12.5 μg mL<sup>-1</sup> tetracycline were used as starting culture. Next day, we prepared a fresh (overday) culture by inoculating 50 μL of overnight culture per mL of LB medium with 100 μg mL<sup>-1</sup> ampicillin, let it grow until OD<sub>600</sub> = 0.8 and seeded 200 μL of the overday culture mixed with IPTG (final concentration 2mM) on NGM plates containing 100 μg mL<sup>-1</sup> ampicillin. The plates were allowed to dry overnight at RT before nematodes were transferred on them. We noticed that the *atp-3* knockdown was extremely toxic, so for our experiments we diluted the overday *atp-3(RNAi)* culture with EV in a 1:1 ratio before seeding.

### Antimycin A treatment

Antimycin A powder (CAS number: 1397-94-0, Sigma-Aldrich) was initially dissolved in 100% EtOH to prepare a 10mM stock solution and stored at -20°C. For every experiment, we prepared a fresh, intermediate 100 μM antimycin A solution, diluted in ddH<sub>2</sub>O. To reach nanomolar concentrations, we further diluted this solution in ddH<sub>2</sub>O and spread it uniformly on the OP50 bacterial lawn on NGM plates. For the majority our experiments with the *p<sub>hsp-6</sub>GFP* reporter we used a final concentration of 50nM antimycin A per NGM plate. The antimycin A-containing NGM plates were allowed to dry before synchronized D1 adult nematodes of the desired genotypes were transferred on them. Day 2 adult animals were microscopically examined 24 h later for *p<sub>hsp-6</sub>GFP* expression.

### ER stress induction

Tunicamycin (CAS number: 11089-65-9, Sigma-Aldrich) was dissolved in DMSO to prepare a 10 mg/mL stock solution. We used a final concentration of 1 μg/mL per NGM plate to trigger ER stress. A tunicamycin solution of the desired concentration was spread uniformly on the OP50 bacterial lawn on NGM plates. The plates were allowed to dry before we transferred synchronized day 1 adult *p<sub>hsp-4</sub>GFP* reporter animals. Day 2 adult animals were microscopically examined 24 h later.

### Heat stress induction

Synchronized day 1 adult *p<sub>hsp-16.2</sub>GFP* reporter animals were transferred in a 37°C incubator for 1 h. The animals were then allowed to recover for 3 h at 20°C before they were anesthetized with tetraisoole (Sigma-Aldrich) and immobilized on agarose pads for microscopic examination.

### Oxidative stress induction

Paraquat (methyl viologen dichloride, CAS number: 75365-73-0, Sigma-Aldrich) was dissolved in ddH<sub>2</sub>O to prepare a 0.5M stock solution. For oxidative stress experiments, we used a final concentration of 1mM paraquat per NGM plate. Synchronized day 1 adult *p<sub>gst-4</sub>GFP* reporter animals were transferred on paraquat-containing NGM plates immediately after they were dry. Day 2 adult animals were microscopically examined 24 h later.

### FUDR treatment

Age-matched L4 larvae were transferred on NGM plates with 100 μM 5-fluoro-2'-deoxyuridine (FUDR, CAS: number 50-91-9, Sigma-Aldrich) for 24 h. D1 adult nematodes were then treated with antimycin A for another 24 h and were microscopically examined at D2 of adulthood.

### Ionizing (IR) and ultraviolet (UV-B) irradiation

For IR experiments, age-matched L4 larvae were irradiated with 120-kV X-rays (25 mA; 0.5mm Alu-filter; ISOVOLT 160 M1/10-55, GE Sensing & Inspection Technologies). For UV-B experiments, age-matched L4 larvae were irradiated with 310-315nm UV-B light using

a narrow band TL01 36-W bulb in a Waldmann UV 181 BL irradiation device. Upon irradiation, the animals were allowed to recover for 24 h before antimycin A challenge.

### Mating

Age-matched wild-type and feminized (*fem-1* mutant) hermaphrodite (XX) L4 larvae were mated with wild-type or *daf-22* mutant males in 35 mm diameter NGM plates in a 1:1 ratio for 24 h. The males were then removed and mated hermaphrodites were transferred on plates seeded with vehicle or antimycin A.

### Western blotting

For the preparation of worm lysates, 100 animals were collected in 25  $\mu$ L of M9 buffer and mixed with an equal volume of 2x SDS sample buffer (125mM Tris pH 6.8, 4% SDS, 4% glycerol, 0.03% bromophenolblue, 50  $\mu$ L/mL  $\beta$ -mercaptoethanol). The samples were boiled at 95°C for 5 min, sonicated in the Bandelin Sonoplus with MS 1.5 sonotrode for 1 min at 60% amplitude, boiled again at 95°C for 5 min and centrifuged at full speed for 10 min. For protein analysis, we performed standard SDS electrophoresis with 12% polyacrylamide gels in a Tris-Glycine-SDS running buffer. We used a semi-dry blotting system (Bio-Rad, Trans-Blot Turbo) for the transfer of proteins to a nitrocellulose membrane (Amersham, Protran 0.2  $\mu$ m). We performed standard transfer with 25 V for 30 min using NuPAGE transfer buffer with a 10% concentration of methanol. After blotting, the membrane was blocked for 1 h (5% milk powder (Carl Roth) in PBS), was washed three times with PBS-Tween (137 mM KCl, 8.1 mM  $\text{Na}_2\text{HPO}_4$ , 1.5 mM  $\text{KH}_2\text{PO}_4$  and 0.1% (v/v) Tween 20, pH 7.4) for 10 min and then incubated with the primary antibody, diluted in PBS-1x Roti-Block (Carl Roth), overnight at 4°C with shaking. We used the anti-living colors monoclonal antibody (JL-8) (Takara Bio, Catalog No.632380) and the anti-alpha tubulin mouse monoclonal, clone B-5-1-2 (Sigma-Aldrich, Product number T5168) as primary antibodies. Both primary antibodies were used in a 1/5000 final concentration. Next day, the membranes were washed three times with PBS-Tween for 10 min. Then, they were incubated with fluorescently labeled secondary antibodies (LI-COR Biosciences) for 1 h at RT, washed again three times with PBS-Tween for 10 min and visualized with the Odyssey scanner (LI-COR Biosciences) and its software (Image Studio Software v5.2, LI-COR Biosciences).

### BioSorter fluorescence quantification

The BioSorter (Union Biometrica) is a large particle flow cytometer, which allows the gating according to parameters such as time-of-flight (TOF) and extinction and quantifies fluorescence in three separate channels 'Green', 'Yellow' and 'Red'. For our experiments, we sorted more than 400 nematodes per condition and used a TOF>1500 to gate only for adult nematodes. The fluorescence measurements are presented as violin plots in [Figure S6E](#).

### Microscopy and image processing

For all our experiments, we anesthetized the worms with 20mM tetramisole hydrochloride (CAS number: [16595-80-5](#), Sigma-Aldrich), mounted them on 2% agarose pads on glass microscopy slides and examined them with a ZEISS Axio Zoom.V16 stereomicroscope and the ZEISS ZEN software. We used the same exposure time (200ms) for the acquisition of all photos. Each microscopy experiment was performed with 10–15 age-matched worms per genotype and condition and was repeated at least three times producing similar results.

### Lifespan assay

Lifespan experiments with the DCL569 strain were performed at 20°C. All mitochondrial RNAi treatments were initiated from hatching. Synchronization was achieved with hypochlorite treatment. The eggs were washed three times with M9 buffer and were immediately spread on RNAi plates with a final concentration of 2mM IPTG. The animals were first transferred three days later (day 1 of adulthood) and then every two days to fresh RNAi plates. From day 5 of adulthood and onwards the plates were examined every day and the animals were scored as alive or dead. Worms that did not respond to a double gentle touch with the worm pick were recorded as dead, whereas those with internally hatched eggs, protruding vulvas, or those that accidentally died due to handling were recorded as censored. The lifespan experiment was repeated independently two times and one representative experiment is shown in [Figure 4F](#).

## QUANTIFICATION AND STATISTICAL ANALYSIS

Mean fluorescence intensity was quantified in regions of interest (ROIs) surrounding the intestine using the Fiji-ImageJ software. We used the GraphPad Prism 8 software package for designing graphs and performing the subsequent statistical analyses. All values in quantification panels are presented as mean  $\pm$  SD and expressed as mean fluorescence intensity normalized to untreated controls. Statistical significance was estimated with one-way or two-way analysis of variance (ANOVA) followed by Sidak's and Tukey's multiple comparison test. The significance was determined by the *p*-values as follows: ns = not significant ( $p > 0.05$ ), \* ( $p < 0.05$ ), \*\* ( $p < 0.01$ ) and \*\*\* ( $p < 0.001$ ).

Cell Reports, Volume 43

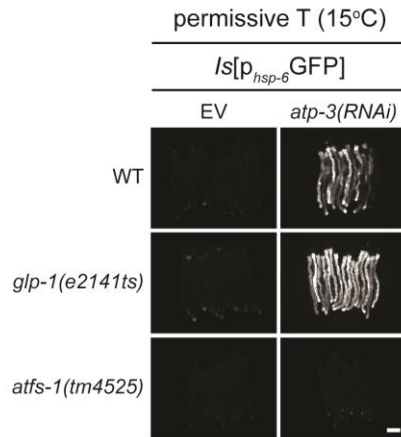
**Supplemental information**

**Reproductive regulation of the mitochondrial  
stress response in *Caenorhabditis elegans***

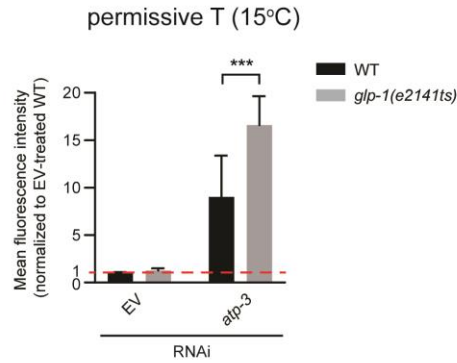
**Nikolaos Charmpilas, Aggeliki Sotiriou, Konstantinos Axarlis, Nektarios  
Tavernarakis, and Thorsten Hoppe**

# Figure S1

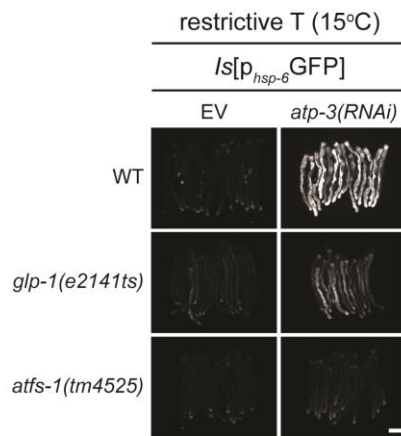
**A**



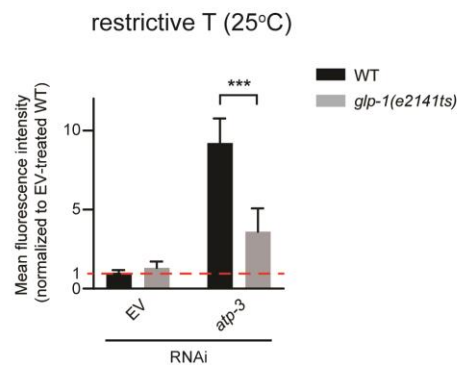
**B**



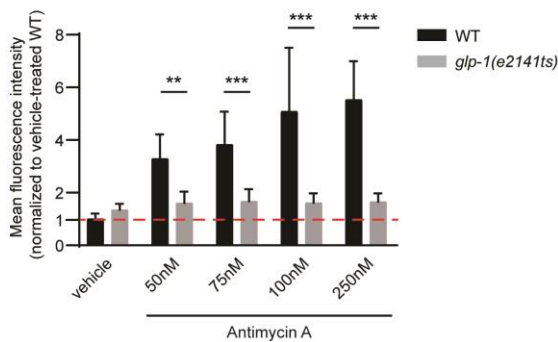
**C**



**D**



**E**



**F**

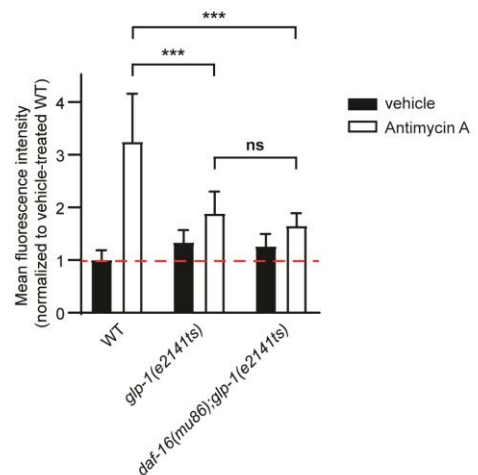


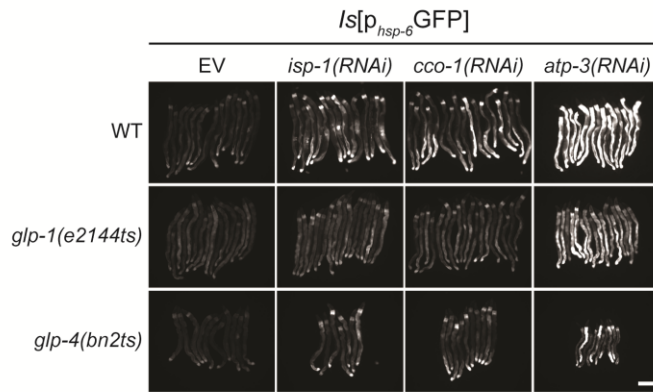
**Figure S1: A temperature-sensitive *glp-1* mutation compromises UPR<sup>mt</sup> inducibility.** Related to Figure 1.

A) Photomicrographs of day 3 adult wild-type (WT) and *glp-1(e2141ts)* mutant p<sub>*hsp-6*</sub>GFP reporter nematodes raised at the permissive temperature (15°C) and treated with empty vector (EV) and *atp-3(RNAi)* from the L4 larval stage. B) Quantification of intestinal p<sub>*hsp-6*</sub>GFP fluorescence in WT and *glp-*

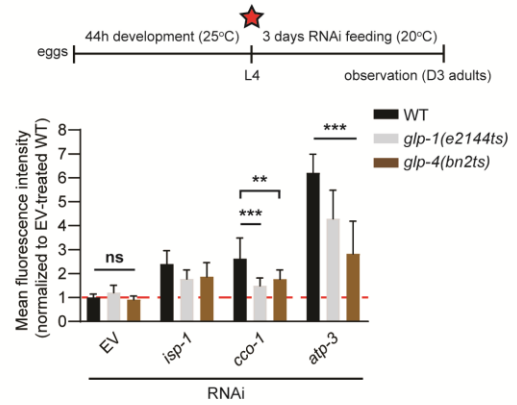
*1(e2141ts)* mutants at the permissive temperature (n=2; \*\*\*p<0.001; two-way ANOVA). C) Photomicrographs of day 3 adult WT and *glp-1(e2141ts)* mutant  $p_{hsp-6}$ GFP reporter nematodes raised at the restrictive temperature (25°C) and treated with empty vector (EV) and *atp-3(RNAi)* from the L4 larval stage. D) Quantification of intestinal  $p_{hsp-6}$ GFP fluorescence in WT and *glp-1(e2141ts)* mutants at the restrictive temperature (n=2; \*\*\*p<0.001; two-way ANOVA). E) Quantification of  $p_{hsp-6}$ GFP fluorescence in WT and *glp-1(e2141ts)* mutants upon treatment with increasing concentrations of antimycin A (n=3; \*\*\*p<0.001, \*\*p<0.01; two-way ANOVA). F) Quantification of  $p_{hsp-6}$ GFP fluorescence in WT, *glp-1(e2141ts)* and *daf-16(mu86); glp-1(e2141ts)* mutants upon treatment with antimycin A (n>3; \*\*\*p<0.001; two-way ANOVA). Data are represented as mean  $\pm$  SD. Scale bars, 200 $\mu$ m.

# Figure S2

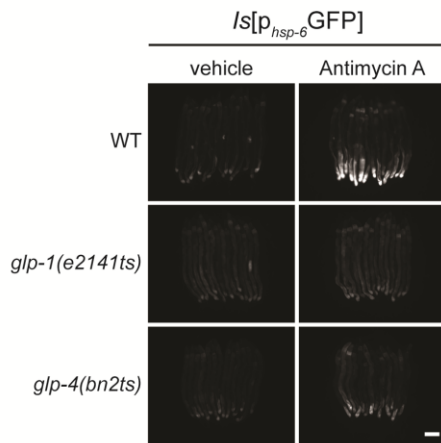
**A**



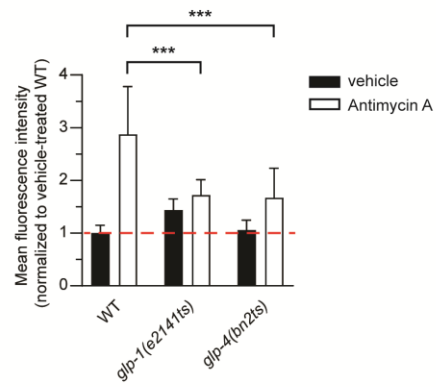
**B**



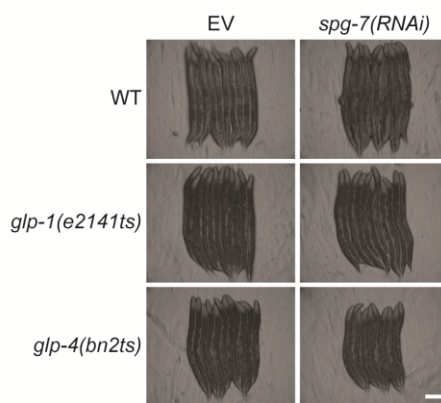
**C**



**D**



**E**



**F**

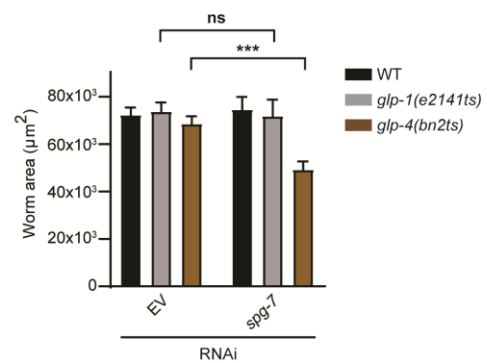


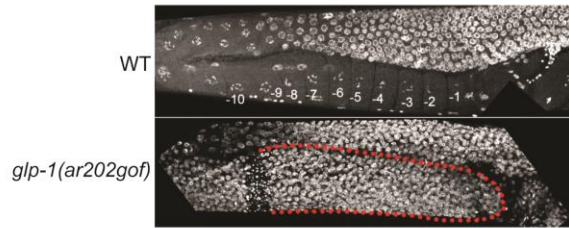
**Figure S2: Germline-less *glp-4* mutants are less responsive and vulnerable to mitochondrial stress.** Related to Figure 1.

A) Photomicrographs of day 3 adult wild-type (WT), *glp-1(e2144ts)* and *glp-4(bn2ts)* mutant  $p_{hsp-6}$ GFP

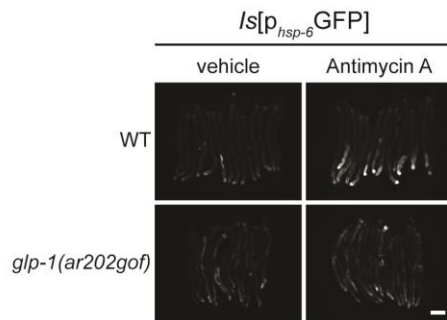
reporter nematodes treated with empty vector (EV) and three UPR<sup>mt</sup>-inducing RNAs from the L4 larval stage. B) Quantification of  $p_{hsp-6}$ GFP fluorescence intensity in WT, *glp-1(e2144ts)* and *glp-4(bn2ts)* mutants (n=3; \*\*\*p<0.001, \*\*p<0.01; two-way ANOVA). C) Photomicrographs of day 2 adult WT, *glp-1(e2141ts)* and *glp-4(bn2ts)* mutant  $p_{hsp-6}$ GFP reporter nematodes treated with antimycin A. D) Quantification of  $p_{hsp-6}$ GFP fluorescence in WT, *glp-1(e2141ts)* and *glp-4(bn2ts)* mutants upon treatment with antimycin A (n=3; \*\*\*p<0.001; two-way ANOVA). E) Photomicrographs of WT, *glp-1(e2141ts)* and *glp-4(bn2ts)* mutants after 72h of feeding with EV or *spg-7(RNAi)* from hatching. F) Quantification of worm surface area (n=2; \*\*\*p<0.001; two-way ANOVA). Data are represented as mean  $\pm$  SD. Scale bars, 200 $\mu$ m.

## Figure S3

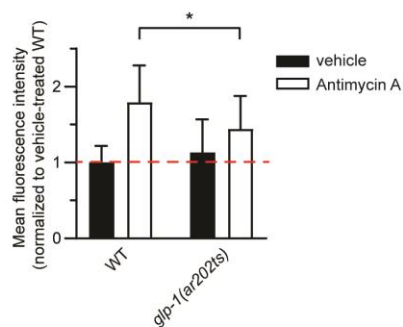
**A**



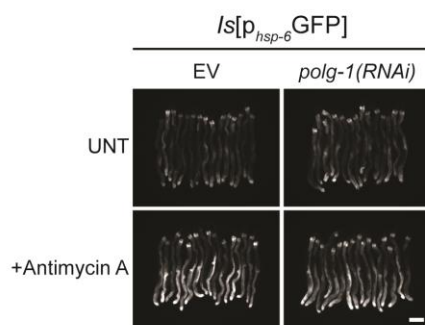
**B**



**C**



**D**



**E**

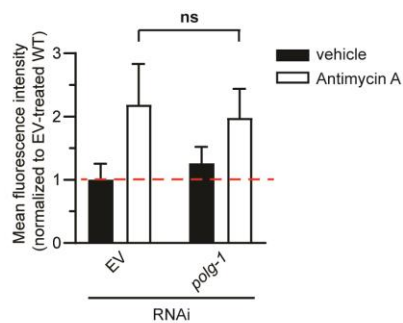


**Figure S3: Inhibition of germline stem cell proliferation and reduced mtDNA copy number cannot explain the reduced somatic UPR<sup>mt</sup> inducibility of germline-less mutants.** Related to Figure 2.

A) DAPI staining of WT and *glp-1(ar202gof)* mutant nematodes. The dashed red line surrounds the mitotic cells formed ectopically in the proximal gonad arm of *glp-1(ar202ts)* mutants. B) Photomicrographs of day 2 adult WT and *glp-1(ar202gof)* mutant  $p_{hsp-6}$ GFP reporter nematodes treated with antimycin A for 24 hours. C) Quantification of  $p_{hsp-6}$ GFP fluorescence in WT and *glp-1(ar202gof)* mutants upon treatment with antimycin A (n=3; \*p<0.05; two-way ANOVA). D) Photomicrographs of day 2 adult  $p_{hsp-6}$ GFP reporter nematodes raised on empty vector (EV) or *polg-1(RNAi)*-expressing bacteria from hatching and treated at day 1 of adulthood with antimycin A for 24 hours. E) Quantification of  $p_{hsp-6}$ GFP fluorescence in EV and *polg-1(RNAi)*-treated  $p_{hsp-6}$ GFP reporter animals upon challenge with antimycin A (n=3; ns p>0.05; two-way ANOVA). Data are represented as mean  $\pm$  SD. Scale bars, 200 $\mu$ m.

# Figure S4

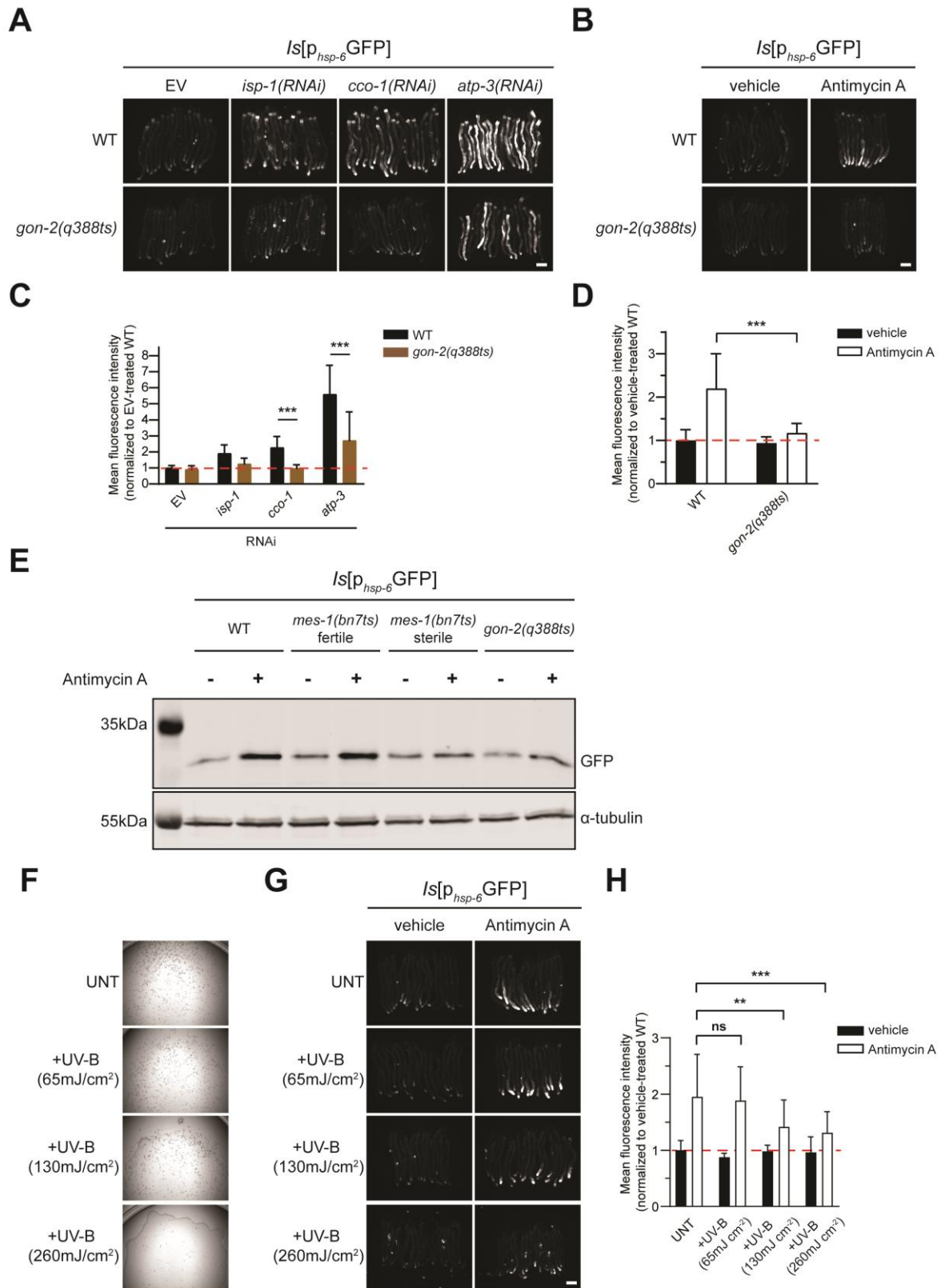


**Figure S4: Inhibition of somatic gonad development and UV-B stress lead to reduced somatic UPR<sup>mt</sup> inducibility.** Related to Figure 2.

A) Photomicrographs of day 3 adult WT and *gon-2(q388ts)* mutant *p<sub>hsp-6</sub>GFP* reporter nematodes treated

with empty vector (EV) and three UPR<sup>mt</sup>-inducing RNAs from the L4 larval stage. B) Photomicrographs of day 2 adult WT and *gon-2(q388ts)* mutant  $p_{hsp-6}$ GFP reporter nematodes treated with antimycin A for 24 hours. C) Quantification of  $p_{hsp-6}$ GFP fluorescence in WT and *gon-2(q388ts)* mutants. Treatments are the same as denoted in (A) (n=3; \*\*\*p<0.001; two-way ANOVA). D) Quantification of  $p_{hsp-6}$ GFP fluorescence in WT and *gon-2(q388ts)* mutants upon antimycin A treatment (n=3; \*\*\*p<0.001; two-way ANOVA). E) Western blot for detecting  $p_{hsp-6}$ GFP in untreated or antimycin A-treated WT, *mes-1(bn7ts)* and *gon-2(q388ts)* mutants.  $\alpha$ -tubulin was used as a loading control. F) Exposure to increasing doses of UV-B radiation leads to reduced brood size. G) Photomicrographs of day 2 adult WT  $p_{hsp-6}$ GFP reporter nematodes exposed to increasing doses of UV-B irradiation prior to the antimycin A challenge. H) Quantification of  $p_{hsp-6}$ GFP fluorescence intensity upon antimycin A challenge in untreated and UV-B-treated worms (n=3; \*\*\*p<0.001, \*\*p<0.01; two-way ANOVA). Data are represented as mean  $\pm$  SD. Scale bars, 200 $\mu$ m.

## Figure S5

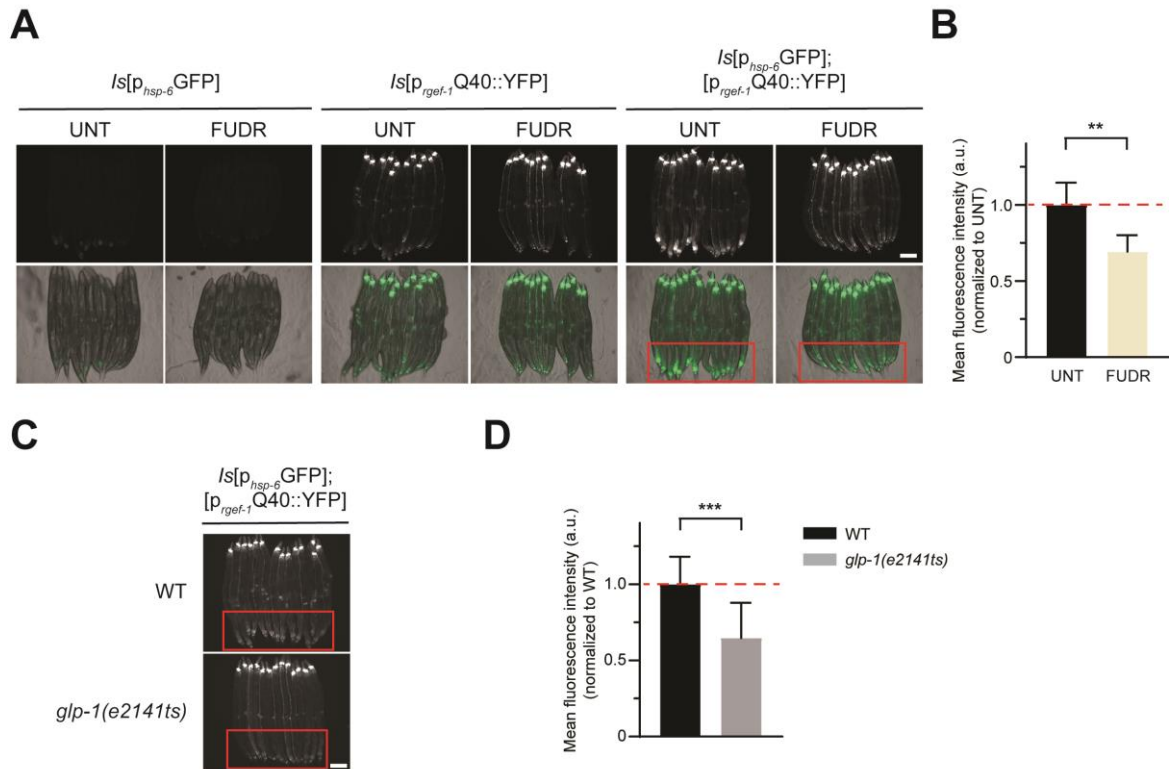
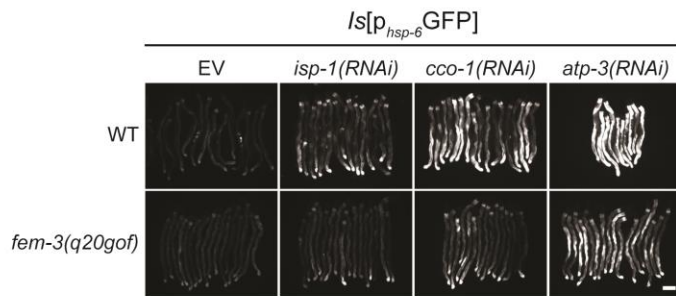


**Figure S5: A proliferating germline is required for cell non-autonomous UPR<sup>mt</sup> induction in response to a panneuronal Q40 polyglutamine tract.** Related to Figure 2.

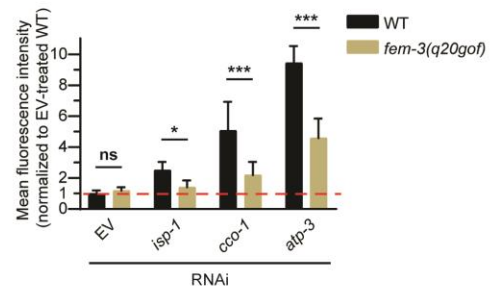
A) Photomicrographs of day 2 adult  $p_{hsp-6}GFP$ ,  $p_{rgef-1}Q40::YFP$  and  $p_{hsp-6}GFP$ ;  $p_{rgef-1}Q40::YFP$  reporter nematodes raised on standard plates or grown on FUDR-containing plates after the L4 larval stage. The red rectangle highlights the posterior intestinal region, where  $p_{hsp-6}GFP$  expression is induced in the presence of panneuronal Q40. B) Quantification of  $p_{hsp-6}GFP$  fluorescence intensity in untreated and FUDR-treated  $p_{hsp-6}GFP$ ;  $p_{rgef-1}Q40::YFP$  reporter animals ( $n=3$ ;  $**p<0.01$ ; two-way ANOVA). C) Photomicrographs of day 2 wild-type and *glp-1(e2141ts)* mutant  $p_{hsp-6}GFP$ ;  $p_{rgef-1}Q40::YFP$  reporter nematodes. D) Quantification of  $p_{hsp-6}GFP$  fluorescence intensity in  $p_{hsp-6}GFP$ ;  $p_{rgef-1}Q40::YFP$  reporter animals in the absence or presence of the *glp-1(e2141ts)* mutation ( $n=3$ ;  $***p<0.001$ ; two-way ANOVA). Data are represented as mean  $\pm$  SD. Scale bars, 200 $\mu$ m.

## Figure S6

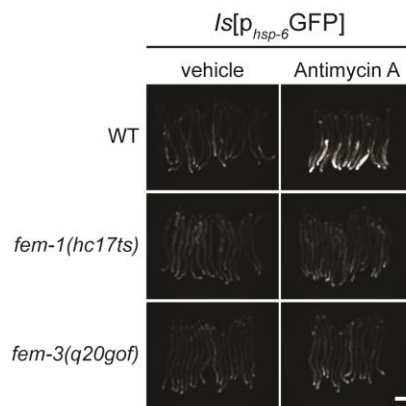
**A**



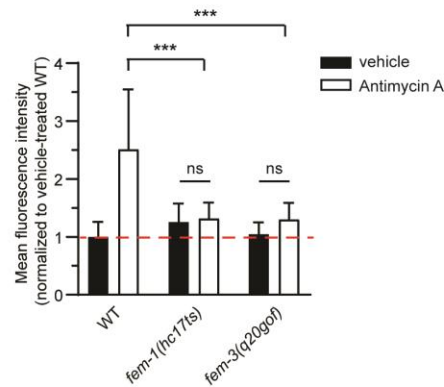
**B**



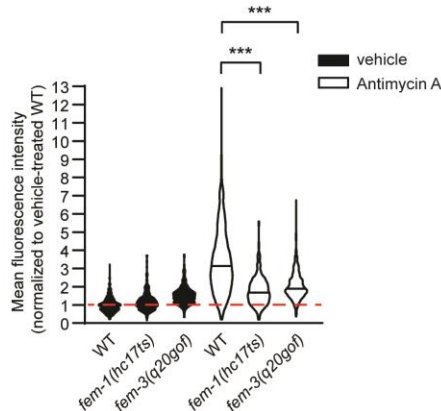
**C**



**D**



**E**



**F**

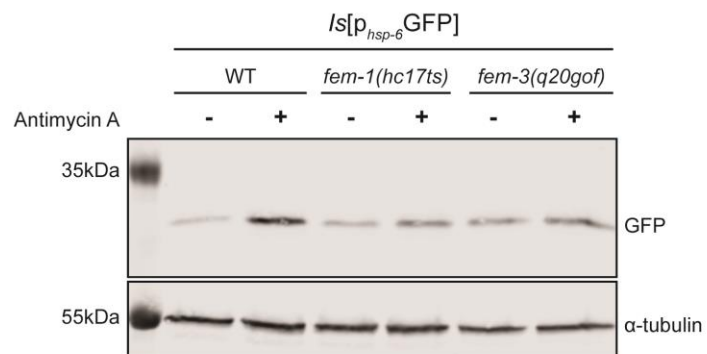
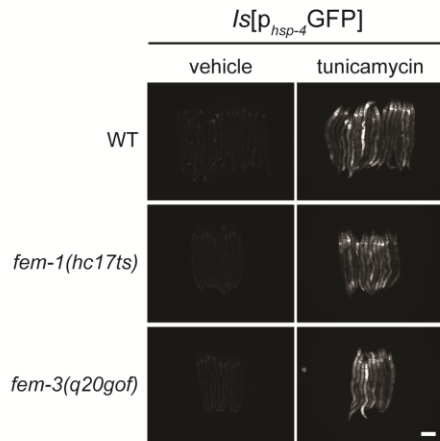


**Figure S6: Active reproduction is indispensable for somatic UPR<sup>mt</sup> induction.** Related to Figure 3. A) Photomicrographs of day 3 adult WT and *fem-3(q20gof)* mutant  $p_{hsp-6}$ GFP reporter nematodes treated with empty vector (EV) and three UPR<sup>mt</sup>-inducing RNAs from the L4 larval stage. B) Quantification of intestinal  $p_{hsp-6}$ GFP fluorescence in WT and masculinized mutants ( $n > 3$ ;  $***p < 0.001$ ,  $*p < 0.05$ ; two-way ANOVA). C) Photomicrographs of day 2 adult WT, *fem-1(hc17ts)* and *fem-3(q20gof)* mutant  $p_{hsp-6}$ GFP reporter nematodes treated with antimycin A for 24 hours. D) Quantification of  $p_{hsp-6}$ GFP fluorescence in WT, *fem-1(hc17ts)* and *fem-3(q20gof)* mutants ( $n > 3$ ;  $***p < 0.001$ ; two-way ANOVA). E) Copas Biosorter quantification of  $p_{hsp-6}$ GFP fluorescence in WT, *fem-1(hc17ts)* and *fem-3(q20gof)* mutant under

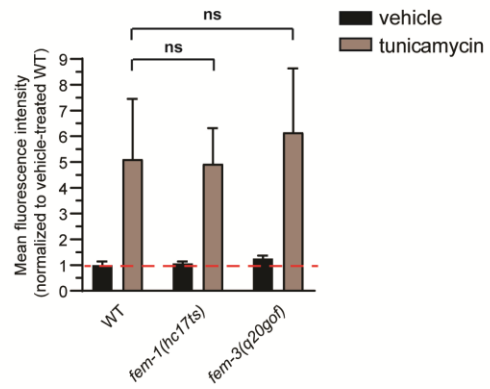
baseline conditions and upon treatment with antimycin A (n=2; \*\*\*p<0.001; two-way ANOVA). F) Western blot for detecting p<sub>hsp-6</sub>GFP in untreated or antimycin A-treated WT, sperm-deficient and oocyte-deficient mutants.  $\alpha$ -tubulin was used as a loading control. Data are represented as mean  $\pm$  SD. Scale bars, 200 $\mu$ m.

# Figure S7

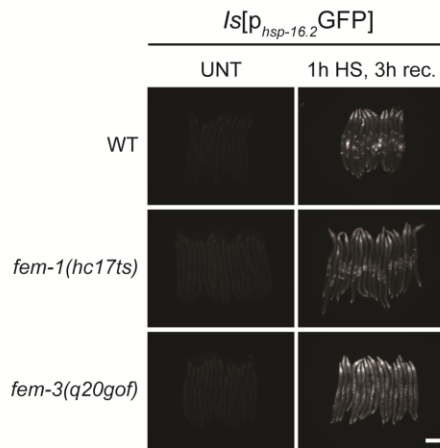
**A**



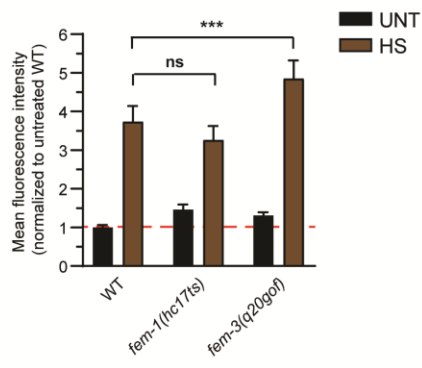
**B**



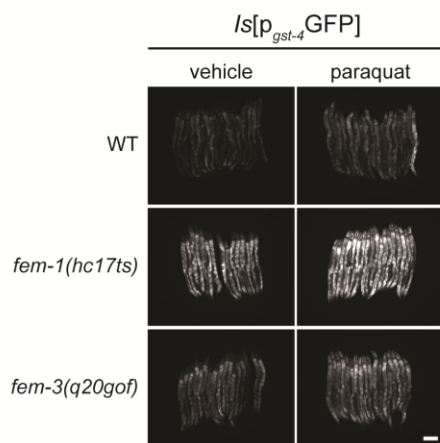
**C**



**D**



**E**



**F**

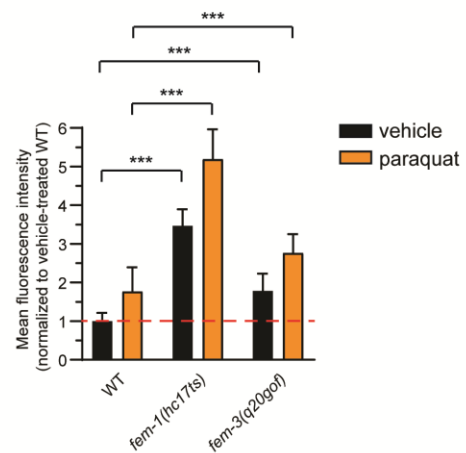


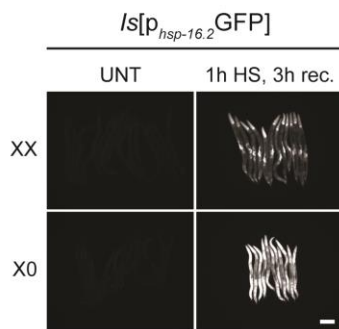
**Figure S7: Sperm- and oocyte-deficient mutants can induce the UPR<sup>ER</sup>, the cytoplasmic HSR and the oxidative stress response.** Related to Figure 3.

A) Photomicrographs of day 2 adult WT, *fem-1(hc17ts)* and *fem-3(q20gof)* mutant  $p_{hsp-4}$ -GFP reporter

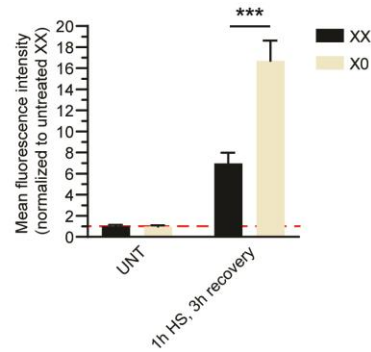
nematodes treated with vehicle or tunicamycin for 24 hours. B) Quantification of  $p_{hsp-4}$ GFP fluorescence in WT, *fem-1(hc17ts)* and *fem-3(q20gof)* mutants (n=3; ns  $p>0.05$ ; two-way ANOVA). C) Photomicrographs of day 1 adult WT, *fem-1(hc17ts)* and *fem-3(q20gof)* mutant  $p_{hsp-16.2}$ GFP reporter nematodes upon 1 hour of heat shock at 37°C followed by a 3-hour recovery. D) Quantification of  $p_{hsp-16.2}$ GFP fluorescence in WT, *fem-1(hc17ts)* and *fem-3(q20gof)* mutants (n=3; \*\*\* $p<0.001$ ; two-way ANOVA). E) Photomicrographs of day 2 adult WT, *fem-1(hc17ts)* and *fem-3(q20gof)* mutant  $p_{gst-4}$ GFP reporter nematodes treated with vehicle or paraquat for 24 hours. F) Quantification of  $p_{gst-4}$ GFP fluorescence in WT, *fem-1(hc17ts)* and *fem-3(q20gof)* mutants (n=3; \*\*\* $p<0.001$ ; two-way ANOVA). Data are represented as mean  $\pm$  SD. Scale bars, 200 $\mu$ m.

## Figure S8

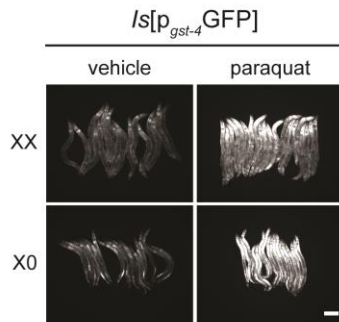
A



B



C



D

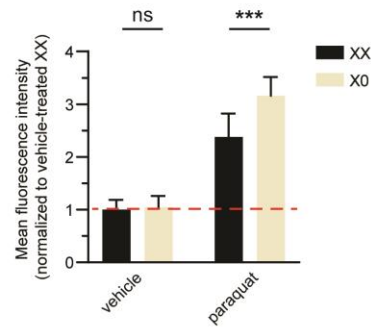
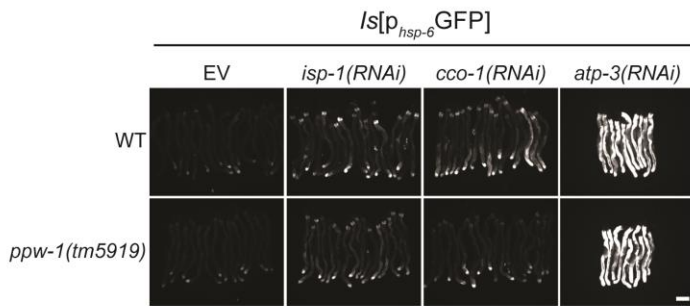


**Figure S8: Male nematodes respond to heat shock and oxidative stress.** Related to Figure 3.

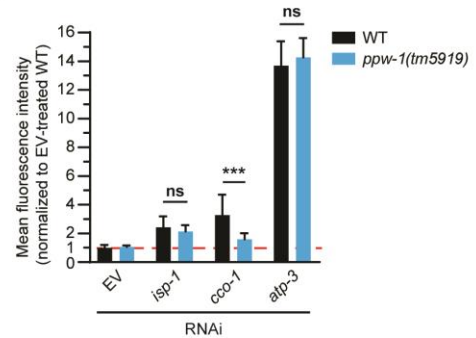
A) Photomicrographs of day 1 adult hermaphrodite (XX) and male (X0)  $p_{hsp-16.2}$ GFP reporter siblings upon 1 hour of heat shock at 37°C followed by a 3-hour recovery. B) Quantification of  $p_{hsp-16.2}$ GFP fluorescence in wild-type day 1 adult hermaphrodites (XX) and males (X0) upon heat shock ( $n=3$ ;  $***p<0.001$ ; two-way ANOVA). C) Photomicrographs of day 2 adult hermaphrodite (XX) and male (X0)  $p_{gst-4}$ GFP reporter siblings upon 24-hour exposure to paraquat. D) Quantification of  $p_{gst-4}$ GFP fluorescence in wild-type day 2 adult hermaphrodites (XX) and males (X0) upon paraquat treatment for 24 hours ( $n=3$ ;  $***p<0.001$ ; two-way ANOVA). Data are represented as mean  $\pm$  SD. Scale bars, 200 $\mu$ m.

## Figure S9

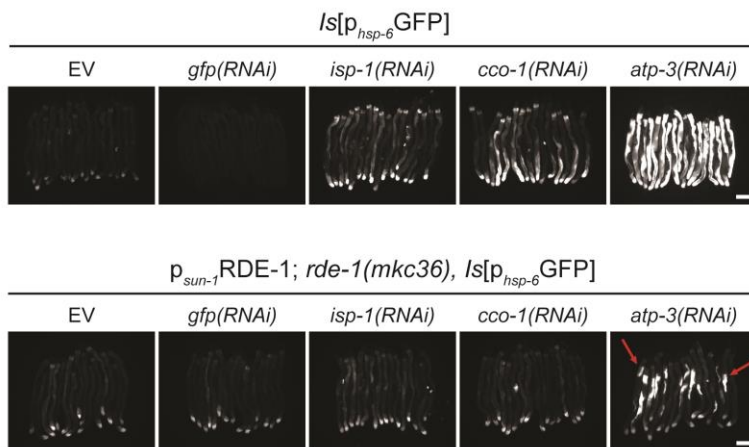
**A**



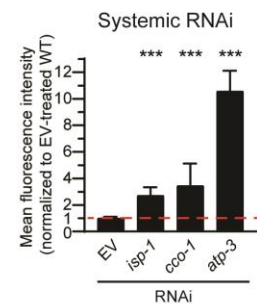
**B**



**C**



**D**



**E**

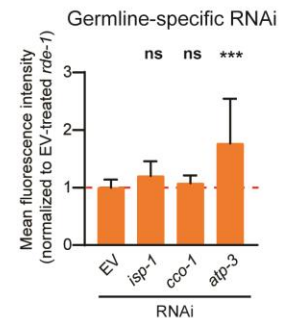


**Figure S9: Germline mitochondrial stress induces UPR<sup>mt</sup> in the soma.** Related to Figure 4.

A) Photomicrographs of day 3 adult WT and  $ppw-1(tm5919)$  mutant  $p_{hsp-6}GFP$  reporter nematodes treated with empty vector (EV), and three UPR<sup>mt</sup>-inducing RNAs for three consecutive days from the L4 stage. B) Quantification of intestinal  $p_{hsp-6}GFP$  fluorescence in WT and  $ppw-1(tm5919)$  mutant  $p_{hsp-6}GFP$  reporter nematodes. Treatments are the same as denoted in (A) (n=2; \*\*\*p<0.001; two-way ANOVA). C) Photomicrographs of day 3 adult wild-type (WT) and  $rde-1(mkc36);p_{sun-1}RDE-1$   $p_{hsp-6}GFP$  reporter nematodes treated with empty vector (EV),  $gfp(RNAi)$  and three UPR<sup>mt</sup>-inducing RNAs for three consecutive days from the L4 stage. The red arrows highlight the induction of  $p_{hsp-6}GFP$  expression in the intestine of  $atp-3(RNAi)$ -treated  $rde-1(mkc36);p_{sun-1}RDE-1$   $p_{hsp-6}GFP$  reporter nematodes. D) Quantification of intestinal  $p_{hsp-6}GFP$  fluorescence in WT  $p_{hsp-6}GFP$  reporter nematodes (n=2; \*\*\*p<0.001; two-way ANOVA). E) Quantification of intestinal  $p_{hsp-6}GFP$  fluorescence in  $rde-1(mkc36);p_{sun-1}RDE-1$   $p_{hsp-6}GFP$  reporter nematodes (n=2; \*\*\*p<0.001; two-way ANOVA). Data are represented as mean  $\pm$  SD. Scale bars, 200 $\mu$ m.

# Figure S10

Figure 4

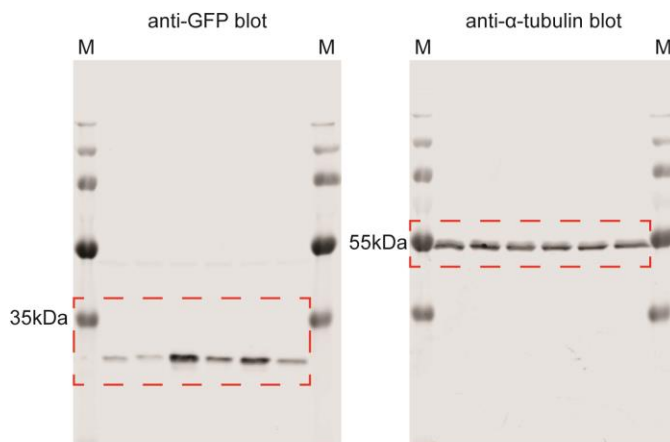


Figure S4

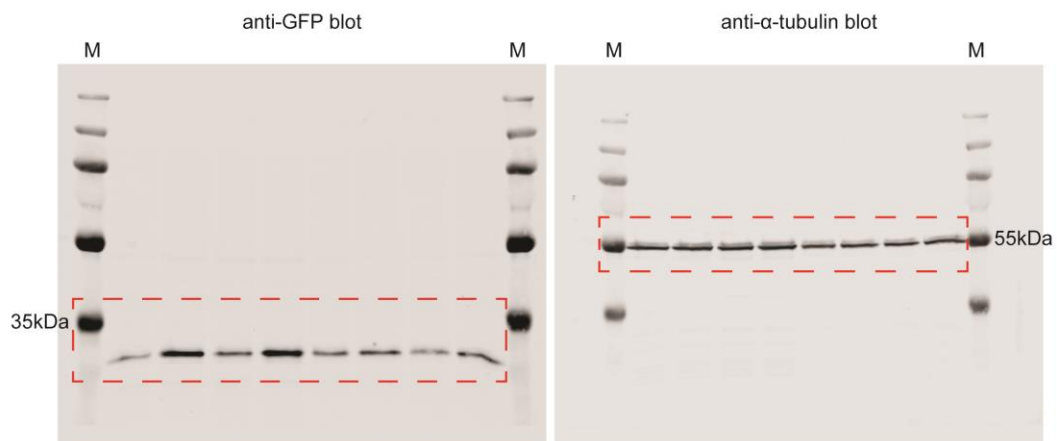
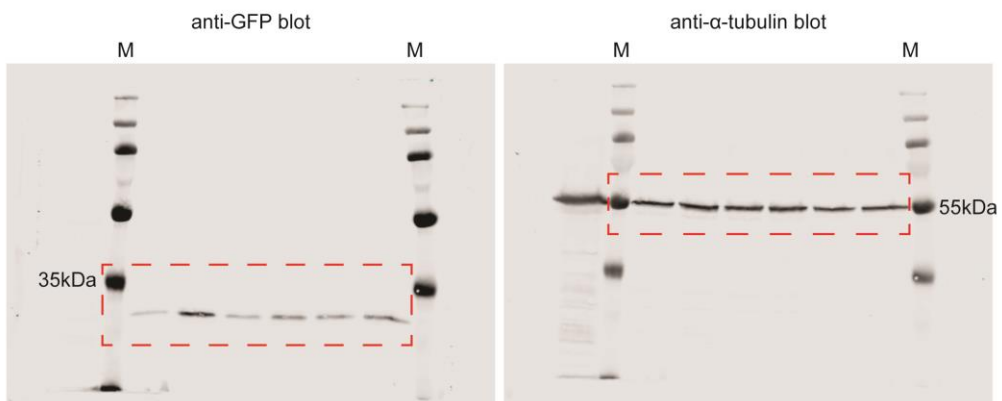


Figure S6



**Figure S10: Uncropped protein gels.** Related to Figure 4, Figure S4 and Figure S6. The red dashed rectangles highlight gel areas that were included in the respective figures.